molecular pharmaceutics

Article

Cite This: Mol. Pharmaceutics 2017, 14, 3644-3659

pubs.acs.org/molecularpharmaceutics

Cleavable Multifunctional Targeting Mixed Micelles with Sequential pH-Triggered TAT Peptide Activation for Improved Antihepatocellular Carcinoma Efficacy

Jinming Zhang,[†,#] Yifeng Zheng,[§,#] Xi Xie,[∥] Lan Wang,[§] Ziren Su,[*,§] Yitao Wang,[†] Kam W. Leong,[⊥] and Meiwan Chen[*,†]

[†]State Key Laboratory of Quality Research in Chinese Medicine, Institute of Chinese Medical Sciences, University of Macau, Macao 999078, China

[§]College of Chinese Medicines, Guangzhou University of Chinese Medicine, Guangzhou 510006, China

[∥]State Key Laboratory of Optoelectronic Materials and Technologies, School of Electronics and Information Technology, Sun Yat-Sen University, Guangzhou 510275, China

[⊥]Department of Biomedical Engineering, Columbia University, New York, New York 10027, United States

ABSTRACT: Although tumor-targeting nanovehicles for hepatocellular carcinoma (HCC) chemotherapy have attracted great research and clinic interest, the poor cancer penetration, inefficient cellular uptake, and slow intracellular drug release greatly compromise their therapeutic outcomes. In this work, a multifunctional mixed micellar system, consisting of glycyrrhetinic acid (GA) for specific liver-targeting, trans-activator of transcription (TAT) peptide for potent cell penetration, and pH-sensitive poly(β-amino ester) polymers for acidic-triggered drug release, was developed to provide HCC-targeting delivery and pH-triggered release of doxorubicin (DOX). These micelles were hypothesized to efficaciously accumulate in HCC site by the guide of GA ligands, enter into cancer cells facilitated by the activated TAT peptide on the micellar surface, and finally rapidly release DOX in cytoplasm. To demonstrate this design, DOX was initially loaded in micelles modified with both GA and TAT (DOX/GA@TAT-M) with high drug loading efficiency and pH-sensitive drug release profiles. The HCC-targeting cellular uptake and synergetic anticancer efficacy were tested, indicating DOX/GA@TAT-M could be specifically and effectively internalized into HCC cells by the effect of GA targeting and TAT penetrating with enhanced cytotoxicity. In addition, the prolonged circulation time and enhanced accumulation in tumor facilitated its potent tumor growth inhibition activity *in vivo*. These results demonstrated that the cleavable multifunctional mixed micelles with tumor targeting, controlled TAT peptide activation, and sequential pH-sensitive drug release could be an efficient strategy for HCC treatment.

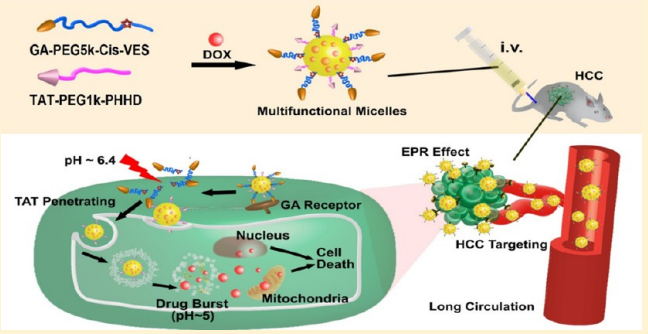

KEYWORDS: *tumor-targeting, glycyrrhetinic acid, pH-sensitive, TAT exposure, mixed micelles*

INTRODUCTION

As the most frequent primary liver cancer, hepatocellular carcinoma (HCC) treatment is in urgent need, yet effective therapeutic options are still lacking.[1] Compared to surgical approaches with limited applicability in major HCC treatment,[2] doxorubicin (DOX) has been accepted by physicians as a feasible drug for advanced HCC treatment.[3] Unfortunately, conventional chemotherapeutic treatment is still suffering from low response rate (<10%) and unclear impact on overall survival.[4] The poor circulation profiles and ineffective delivery to tumor site are the primary limiting steps.

Nanoparticle therapeutics have emerged as powerful tools for enhancing clinical outcome while simultaneously reducing undesirable side-effects.[5,6] Particularly, engineering multifunctional nanocarriers based on specific tumor receptor targeting with stimuli-responsive properties can significantly offer potential advantages over conventional nontargeted chemotherapy.[7−9] Receptor-targeted nanocarriers by conjugation of targeting ligands onto vehicles can selectively deliver cargoes to cancer cells or vasculature site, thereby facilitating efficient drug accumulation in the target site.[6] A variety of ligands, including antibodies, peptides, and aptamers, and small molecules, such as folate, have been employed for tumor targeting.[10,11] In particular, glycyrrhetinic acid (GA), the main compound of liquorice, has demonstrated specific liver-targeting capacity through binding to protein kinase C, which is overexpressed on cellular membrane of hepatocyte, especially cancerous

Received: May 15, 2017
Revised: September 3, 2017
Accepted: September 8, 2017
Published: October 10, 2017

DOI: 10.1021/acs.molpharmaceut.7b00404
Mol. Pharmaceutics 2017, 14, 3644−3659

hepatocytes.[12,13] The application of GA as liver-targeting ligand onto nanocarrier has attracted increasing research interest, due to its few immune-reaction and stable receptor-expression.[14−16] Although enhanced accumulation of drugs by conjugating nanocarrie with GA ligand in liver cancer cells has been found *in vitro* in previous studies, how to effectively cross the vascular wall and penetrate into the solid tumor parenchyma against the elevated interstitial pressure in tumors remains challenging.[17−19] Moreover, the receptor−ligand recognition pathway-mediated endocytosis cannot provide adequate transport of ligand-conjugated cargoes into cancer cells due to the accustomed receptor saturation.[20,21]

Cell-penetrating peptides provide a promising approach to promote intracellular drug delivery by its advantage to easily facilitate cargoes transportation through cell membranes.[22−24] In particular, human immunodeficiency virus type-1 transcription transactivator (TAT) peptide has been explored as an effective tool for cancer penetration.[25] Although TAT functionalized nanoparticles (NPs) have opened up potential avenues for improved drug delivery,[26] their non-tissue specificity and instability due to binding with opsonin in the blood circulation prevent them from clinical applications.[27,28] Recent attempts on the fabrication of activatable TAT-functionalized NPs with PEG surface modification have achieved reasonable success on prolonged circulation *in vivo*, and these NPs were triggered to expose in tumor extracellular space by external stimulus, such as redox, pH, or matrix metallo proteinase.[29−32]

In this work, a cleavable multifunctional micelle system with the combination of tumor targeting ability of GA ligands, the transmembrane function of TAT, and pH-sensitive drug release was developed. A pH-sensitive poly(β-amino ester) polymer, poly [(1,6-hexanediol)-dia-crylate-β-6-hexylenediamime)] (PHHD), was synthesized as the encapsulation domain for DOX. This polymer was designed to be pH-responsive in order to facilitate intracellular release and endosomal escape of the loaded DOX. TAT with effective transmembrane function was conjugated to PHHD−PEG_{1000} copolymer (TAT-PEG_{1k}-PHHD), which serves as the interlayer of the micelle. GA ligands with target selectivity were functionalized on another pH-detachable longer polymer, PEG_{5000}-cis-acotonic anhydride-vitamin E succinate ($P_{5k}CV$), which serves as the external layer of the delivery vehicles. The TAT ligands were designed to be embedded in the interlayer to minimize the undesirable side-effects resulted from their positive charges. We hypothesized these functional micelles could effectively improve anti-HCC capacity by the following synergistic approaches: (i) Initially, the enhanced permeability and retention (EPR) effect and GA-receptor mediated HCC-targeting make micelles apt to accumulate at the HCC site. (ii) Along with the external PEG_{5000} layer breakage by pH-responsive hydrolysis of cis-acotonic anhydride linkage (pH ≈ 6.4), TAT peptides in the interlayer were exposed and facilitated tissue/cell penetration of the micelles. (iii) Finally, PHHD as the acid-sensitive polymeric domain could be rapidly disintegrated in the endo/lysosomal environment (pH < 6), with improved nuclear delivery of DOX. These DOX-loaded multifunctional micelles were demonstrated that HCC-targeting, enhanced cell penetration, and pH-sensitive drug release can achieve the improved anti-HCC effects both *in vitro* and *in vivo*, providing a new opportunity for effective cancer therapy with less side-effects.

EXPERIMENTAL SECTION

Materials. Doxorubicin hydrochloride (DOX·HCl, purity ≥98%) and 18α-glycyrrhetinic acid (GA, purity ≥98%) were obtained from Melonepharma Co. Ltd. (Dalian, China) and Jinzhu Pharmaceutical Co., Ltd. (Nanjing, China), respectively. NH_2-PEG_{1k}-COOH and NH_2-PEG_{5k}-NH_2 were purchased from Xibao Biotechnology Co., Ltd. (Shanghai, China). Cis-aconitic anhydride (CAA), dicyclohexylcarbodiimide (DCC), *N*-hydroxy-succinimide (NHS), 4-dimethylaminopyridine (DMAP), and 1-ethyl-3-(3-(dimethylamino)propyl) carbodiimide hydrochloride (EDC) were obtained from GL Biochem Co. Ltd. (Shanghai, China). TAT peptide with a terminal amino group (Tyr-Gly-Arg-Lys-Lys-Arg-Arg-Gln-Arg-Arg-Arg, purity >95%) was custom-made by GL Biochem Co. Ltd. (Shanghai, China). 1,6-Hexanediol diacrylate (HDDC) and 1,6-hexylenediamime (DMH) were obtained from J&K China. 2,2-Bis(acryloyloxy-methyl) propionic acid (BAP) was synthesized by 2,2-bis (hydroxymethyl) propionic acid and acryloyl chloride in the presence of trimethylamine as previously reported.[33] Vitamin E succinate (VES) was purchased from Sigma-Aldrich (USA). All other chemicals were of analytical grade and used as received. DMEM medium and trypsin without EDTA were obtained from Gibco BRL Co.Ltd. (Gaithersburg, MD, USA). MTT (3-(4,5-dimethylthiazol-2-yl)-2,5-diphenyltetrazolium bromide) was obtained from Biosharp (Seoul, South Korea). Hoechst 33342 was obtained from Life Technologies (Thermo Fisher Scientific, USA). 5,5,6,6-Tetrachloro-1,1,3,3-tetraethyl-benzimidazolylcarbocyanine iodide (JC-1) kit was purchased for mitochondrial membrane potential assay from KeyGen BioTECH (Nanjing, China).

Human hepatocellular liver carcinoma HepG2 cells and SMMC 7721 cells were obtained from American Type Culture Collection (ATCC, Manassas, VA, USA) and grown in DMEM containing 10% fetal bovine serum (FBS), 2 mM L-glutamine, and penicillin-streptomycin (PS) solution at 37 °C in a humidified CO_2 (5%) incubator. BALB/c nude mice, aged 4−6 weeks (18−22 g), were supplied by the animal center of Guangzhou University of Traditional Chinese Medicine and kept under a 12 h light/dark cycle. The animals were acclimatized for at least 7 days prior to the experiments and given a fresh diet with free access to water. All *in vivo* experiments were carried out under the guidelines approved by the Institutional Animal Care and Use Committee (IACUC) of Guangzhou University of Traditional Chinese Medicine.

Synthesis of GA-PEG_{5k}-cis-Aconitic Anhydride-Vitamin E Succinate (GA-P_{5k}CV). GA-PEG_{5k}-cis-aconitic anhydride-vitamin E succinate (GA-P_{5k}CV) was synthesized by three steps: (i) The GA-PEG_{5k}-NH_2 polymer was first synthesized according to our previous study via the amidation reaction between NH_2-PEG_{5k}-NH_2 and activated carboxyl of GA in the presence of EDC, NHS, and triethylamine with a molar ratio of 1:1:1.5:1.5:3. (ii) GA-PEG_{5k}-NH_2 (480.0 mg, 0.1 mmol) was then added successively to a mixture of CAA (15.6 mg, 0.1 mmol), EDC (38.2 mg, 0.2 mmol), and NHS (23 mg, 0.2 mmol) in pyridine. After 24 h of mild stirring with N_2 protection, a crude GA-PEG_{5k}-cis-aconitic anhydride product was obtained from precipitation in cold diethyl ether. (iii) Next, under a nitrogen environment, GA-PEG_{5k}-cis-aconitic anhydride was conjugated with VES using 1,6-hexylenediamine as a linker. GA-PEG_{5k}-cis-aconitic anhydride (300 mg, 0.06 mmol), EDC (19.6 mg, 0.1 mmol), NHS (11.5 mg, 0.1 mmol), and 1,6-hexylenediamine (11.6 mg, 0.1 mmol) were added in anhydrous

DOI: 10.1021/acs.molpharmaceut.7b00404
Mol. Pharmaceutics 2017, 14, 3644−3659

DMF (10 mL) with stirring. The reaction was proceeded for another 24 h at room temperature. The product was further purified by DEAE Sephadex A-25 column chromatography. The GA-P_{5k}CV polymer was obtained by a similar amidation reaction between the residual terminal NH_2 group of GA-PEG_{5k}-cis-aconitic anhydride-hexylenediamine and VES. The resulting GA-P_{5k}CV conjugate was purified by dialysis against a MWCO of 1k and isolated twice by precipitation in cold diethyl ether. The GA-P_{5k}CV fractions were collected and freeze-dried. The final yield rate relative to PEG_{5k} was approximately 59.5%. A Varian Unity-Plus 400 NMR spectrometer (Varian, Inc., USA) was used to verify its structure.

Synthesis of TAT-PEG_{1k}-PHHD. TAT-PEG_{1k}-Poly [(1,6-hexanediol)-diacrylate-β-6-hexylenediamime)] (TAT-PEG_{1k}-PHHD) was synthesized by a three-step procedure: (i) TAT-NH_2 (77.8 mg, 0.05 mmol) was first conjugated to amine PEG carboxylic acid (NH_2-PEG_{1k}-COOH) (100 mg, 0.1 mmol) via amidation reaction in the presence of EDC (19.6 mg, 0.1 mmol) and NHS (11.5 mg, 0.1 mmol) under mild stirring. Thin-layer chromatography (TLC) was utilized to monitor the reaction. For another 16 h, the mixture was placed in a dialysis tube with a MWCO of 1000 to dialyze against deionized water. TAT-PEG_{1k}-NH_2 was obtained by freeze-drying. (ii) Subsequently, TAT-PEG_{1k}-NH_2 lyophilized powder was added dropwise into a dichloromethane (DCM) solution containing carboxylated BAP, EDC, and NHS with molar ratio of 1:1.2:2:2 and reacted for 24 h. The reaction mixture was then filtered and precipitated in an excess of ether. The white TAT-PEG_{1k}-BAP product was vacuum-dried for 24 h. (iii) TAT-PEG_{1k}-PHHD was finally synthesized by Michael addition polymerization using HDDC, DMH and TAT-PEG_{1k}-BAP with a molar ratio of 1:1:0.05. The mixture was placed in a 50 °C water bath for 72 h. The solution was cooled to room temperature and dialyzed against DMSO in a dialysis tube with a MWCO of 7 k for 12 h to remove unreacted monomers. TAT-PEG_{1k}-PHHD copolymer (yield: 78.6%) was obtained by dialysis and followed freeze-drying.

The TAT grafting on the TAT-PEG_{1k}-PHHD copolymer was detected by HPLC with 0.1% trifluoroacetic in 100% acetonitrile: 0.1% trifluoroacetic in 100% water (30:70, v/v) as the mobile phase at the wavelength of 220 nm. As measured by gel permeation chromatography (GPC) with tetrahydrofuran (THF) as the mobile phase, the Mn of the TAT-PEG_{1k}-PHHD copolymer was 31.6k Da, with a polydispersity index (PDI) of 1.79. The structure of the TAT-PEG_{1k}-PHHD copolymer was further characterized by ^{1}H NMR at 400 MHz using deuterated chloroform ($CDCl_3$) as the solvent.

Preparation of DOX-Loaded Mixed Micelles. DOX-loaded mixed micelles were prepared by a pH-induced self-assembly method. Briefly, 30 mg of mixed copolymers of GA-P_{5k}CV and TAT-PEG_{1k}-PHHD at various ratios (w/w) were dissolved in methanol by vortex mixing for 30 s. The mixed polymer solution was gradually injected into 2 mL of PBS (pH 7.4) with a syringe and stirred with 300 rpm at room temperature for 10 min. DOX·HCl aqueous solution (5 mg/mL) was then added dropwise into the polymer mixture and transferred to dialysis tube with MWCO of 3.5 kDa. The mixture was dialyzed against PBS buffer (pH 7.4) for 4 h. DOX loaded in dual-functional micelles (DOX/GA@TAT-M) were obtained, after which free DOX crystals were removed by filtration through a 0.45 μm filter membrane. Similarly, DOX loaded in non-GA modified micelles (DOX/nonGA@TAT-M) were also prepared. Blank mixed micelles were similarly prepared in the absence of DOX.

Physicochemical Characteristics of Mixed Micelles. *pH-Sensitivity and Stability of Micelles.* The particle size and zeta potential of the prepared micelles were determined by dynamic light scattering (DLS) using a Malvern Zetasizer Nano ZSP instrument (Malvern instruments Ltd. U. K.). The pH sensitivity was evaluated by monitoring particle size and zeta potential changes at a series of pH values (7.4, 7.0, 6.8, 6.4, 6.0, and 5.0). The micelle morphology at pH 7.4 was also confirmed by a transmision electron microscopy (TEM) (Tecnai G20, FEI, Hillsboro, OR, USA) at an accelerating voltage of 200 kV. Furthermore, stability of micelles in pH 7.4, 6.4, 5.0 for 7 days storage at room temperature (25 ± 2 °C) was carried out by particle size measurement.

DOX Loading and pH-Sensitive Release in Vitro. The loaded DOX was determined by a Waters e2695 HPLC with a reverse-phase C_{18} column (250 × 4.6 mm, 5 μm) at a maximum absorbance of 490 nm. The mobile phase was composed by acetonitrile and 0.05% acetic acid (26:74, v/v). The drug loading efficiency (DLE%) and drug encapsulation efficiency (DEE%) of DOX in the micelles were calculated by the following equations:

$$\text{DLE\%} = \frac{\text{Amount of drug in micelles}}{\text{Amount of feeding polymer and drugs}} \times 100\% \quad (1)$$

$$\text{DEE\%} = \frac{\text{Amount of drug in micelles}}{\text{Amount of feeding drugs}} \times 100\% \quad (2)$$

The pH-sensitive release kinetics of DOX from DOX/GA@TAT-M *in vitro* were determined by dialysis at pH 7.4, 6.4, and 5.0. Briefly, 2 mL of DOX/GA@TAT-M containing 0.1 mg/mL of DOX were placed in dialysis tubes with a 3.5-kDa MWCO and dialyzed against 40 mL of PBS (pH 7.4, pH 6.4, and pH 5.0) containing 0.5% Tween 80. Drug-release profiles were determined in a 37 °C shaking incubator with a rotation speed of 100 rpm. At predetermined time intervals, 2 mL of dialysis medium was sampled and replaced with 2 mL of prewarmed fresh medium. The released DOX was measured by HPLC after filtration through a 0.22-μm membrane. The release studies were carried out in triplicate.

X-ray Diffraction and Differential Scanning Calorimetry. The crystallographic structures of DOX, lyophilized blank micelles, the physical mixture of DOX and blank micelles (2.5:20, w/w), and lyophilized DOX/GA@TAT-M were characterized by X-ray diffraction (XRD) (Bruker Optik GmbH, Ettlingen, Germany). Samples were exposed to Cu-Ka radiation (40 kV; 40 mA) at a scan rate of 0.016°/second over the 2θ/min range of 5 °C ~ 60 °C.

A diamond differential scanning calorimetry (DSC) (PerkinElmer Inc., Waltham, MA, USA) was employed to detect the thermodynamic properties of samples, including DOX, blank micelles, a physical mixture of DOX and blank micelles (2.5:20, w/w), and lyophilized DOX/GA@TAT-M. The samples were placed in sealed aluminum crimp cells, and heated from 30 to 300 °C at a rate of 5 °C/min.

Cellular Uptake Study. *Cellular Uptake Studied by Flow Cytometry.* The cellular uptake of DOX/GA@TAT-M was evaluated by flow cytometry (FCM) in two cell lines with high levels of GA receptor expression: HepG2 cells and SMMC-7721 cells. Briefly, cells were seeded on a 6-well plates at a density of 20k/well for 24 h to allow adhesion.

DOI: 10.1021/acs.molpharmaceut.7b00404
Mol. Pharmaceutics 2017, 14, 3644−3659

Cells were treated with 1 mL of fresh FBS-free medium containing... at a equivalent DOX concentration of 0.5uM. Moreover, to investigate the uptake under pH-triggered TAT exposure, culture medium with micelle samples was preadjusted to pH 6.4. After an additional incubation for predetermined time periods (1, 2, and 4 h) at 37 °C, the cells were washed twice with cold PBS (pH 7.4), collected by 0.05% trypsin digestion, and washed twice with cold PBS. The cells were resuspended in PBS and analyzed by FCM in the PI fluorescence channel. All operations were carried out in the dark. The fluorescent intensity of the untreated cells was used as the baseline. The amount of cellular uptake was defined as the ratio of the fluorescent intensity of treated cells relative to control cells.

Cellular Mechanisms Investigation. Uptake by SMCC 7721 cells seeded at 1×10^5 cells/well was monitored at 4 °C, following pretreatment with endocytosis inhibitors at 37 °C, or in the presence of free GA at pH 7.4 or pH 6.4. Briefly, SMMC 7721 cells were exposed to free DOX, DOX/GA@TAT-M or DOX/non GA@TAT-M at an equivalent DOX concentration (0.5 μM) for 4 h at 4 and 37 °C respectively. Alternatively, the cells were pretreated with inhibitors for 0.5 h at the following concentrations: GA 1 μM, 2-deoxyglucose 20 mM, chlorpromazine 10 μM, genistein 50 μM, methyl-β-cyclodextrin 5 mM, and wortmannin 10 μM. Afterward, cells were washed three times with cold PBS and subsequently incubated with DOX formulations at 4 and 37 °C. After a 4-h incubation, the cells were washed and collected and intracellular DOX was determined by FCM (Becton Dickinson FACS Canto, Franklin Lakes, NJ, USA).

Internalization Observation. DOX internalization in SMMC 7721 cells was visualized by fluorescence microscopy. As described above, SMMC 7721 cells were incubated with DOX formulations at 37 °C for 4 h at either pH 7.4 or pH 6.4. Moreover, the internalization was evaluated for DOX/GA@TAT-M at 4 °C and pH 6.4, as well as at 37 °C with or without GA pretreatment at pH 7.4. At the end of the incubation period, culture medium was removed. Cells were carefully washed by PBS, fixed with 4% paraformaldehyde for 10 min, stained with Hoechst 33342, and imaged using an InCell Analyzer 2000 (GE Healthcare, USA). Intracellular Hoechst 33342 and DOX were excited using the DAPI and Cy3 fluorescence channels, respectively.

Cytotoxicity Assay. The cytotoxicity of DOX/GA@TAT-M in HepG2 cells and SMMC 7721 cells was evaluated by MTT assay. Briefly, cells were seeded into 96-well plates at 5×10^3 cells/well in DMEM supplemented with 10% FBS. After 24 h adherence, the culture medium was replaced with fresh medium (pH 7.4 or 6.4) containing free DOX, DOX/nonGA@TAT-M, or DOX/GA@TAT-M. After a further incubation for 24 and 48 h, the cells were washed and treated by MTT dye (5 mg/mL) for 4 h to form formazan crystals. And then, DMSO was added to dissolve formazan crystals, and the absorbance was measured at 570 nm using a microplate reader. The IC_{50} values were calculated using GraphPad Prism 6 software.

Mitochondrial Membrane Potential (MMP) Assay. The MMP was analyzed by JC-1 kit. HepG2 and SMMC 7721 cells (5×10^4 cells/well) were harvested after 12 h of exposure to free DOX, DOX/nonGA@TAT-M, or DOX/GA@TAT-M with 0.5 μM DOX at pH 7.4 or pH 6.4 and centrifuged for 5 min at 500 × g. The cells were resuspended in 0.5 mL of JC-1 solution (10 μg/mL) for 20 min. The cells were then washed with PBS buffer, and the fluorescence was detected by FCM. Mitochondrial depolarization is defined as the ratio of (fluorescence $_{red/green}$) treatment/ (fluorescence $_{red/green}$) control.

Similarly, SMMC 7721 cells seeded in 96-well plates were exposed to free DOX, DOX/nonGA@TAT-M, or DOX/GA@TAT-M with 0.5 μM DOX for 12 h. The cells were then washed twice with PBS, and the mitochondrial depolarization of the SMMC-7721 cells was observed on an In Cell Analyzer 2000. Mitochondrial depolarization of apoptotic cells results in the release of JC-1 dye from the mitochondria, which can be observed as a green color. Therefore, red and green coloration represent normal and early apoptotic cells, respectively.

Measurement of Intracellular Reactive Oxygen Species (ROS). ROS amount was detected using the fluorescent probe 5-(and-6)-chloromethyl-2′,7′-dichlorodihydrofluorescein diacetate (DCFH-DA, Life Technologies). SMMC 7721 cells (5.0×10^4/well) were seeded in 6-well plates. After adherence, the cells were incubated with medium containing DOX formulations with equivalent concentrations of DOX (0.5 μM) at pH 7.4 or pH 6.4 for 12 h. The cells were then incubated with 1 μM DCFH-DA for 30 min at 37 °C. After washed three times with cold PBS, cellular ROS production was detected via FCM. The obtained values were expressed as the fold-change with respect to untreated controls.

Apoptosis Analysis by Annexin-V FITC Staining. Cell apoptosis was determined by Annexin V-fluorescein isothiocyanate (FITC)/ Propidium iodide (PI) double staining assay kit (BioVision Inc., San Francisco, USA). SMMC 7721 cells were treated with DOX formulations with equivalent concentrations of DOX (0.5 μM) at pH 7.4 or pH 6.4 for 24 h. Subsequently, cells were harvested, washed with PBS, and resuspended in 100 μL binding buffer containing 5 μL of PI solution and 3 μL of Annexin V-FITC for 15 min. Finally, each sample was analyzed via FCM.

Pharmacokinetics and Biodistribution *in Vivo*. A HCC xenograft mouse model was established via subcutaneous inoculation of 2×10^6 SMMC 7721 cells suspended in saline and matrigel (1:1, v/v) into the left axilla of mice. When the tumor size reached approximately 1000 mm^3, tumor-bearing mice were randomly assigned into three groups ($n = 6$ for each group). To assess the pharmacokinetics and biodistribution of DOX/GA@TAT-M, mice were administrated with a single dose of free DOX, DOX/nonGA@TAT-M, or DOX/GA@TAT-M at an equivalent DOX dose of 5 mg/kg via tail vein. At various intervals post injection, blood was collected in heparinized tubes. Finally, the mice were sacrificed by isoflurane inhalation. Tumor and heart tissues of each mouse were collected, weighed, and homogenized in PBS. Daunorubicin was used as the internal standard.

The amounts of DOX and daunorubicin in plasma samples were determined via liquid chromatography−mass spectrometry (LC/MS) (Q-trap@5500, AB SCIEX, Framingham, MA, USA) in positive ion mode at m/z 544.1 → 397.2 and 528.2 → 321.1, respectively. The mass spectrum conditions were as following: spray voltage at 4500 V, source temperature at 300 °C. The declustering potential and collision energy voltages were set at 60 and 20 V, respectively.

Tumor Accumulation Imaging *in Vivo* and *ex Vivo*. To visualize tumor accumulation in liver-tumor-bearing mice, free DOX, DOX/nonGA@TAT-M, and DOX/GA@TAT-M, with an equivalent DOX dose of 5 mg/kg, were intravenously

DOI: 10.1021/acs.molpharmaceut.7b00404
Mol. Pharmaceutics 2017, 14, 3644−3659

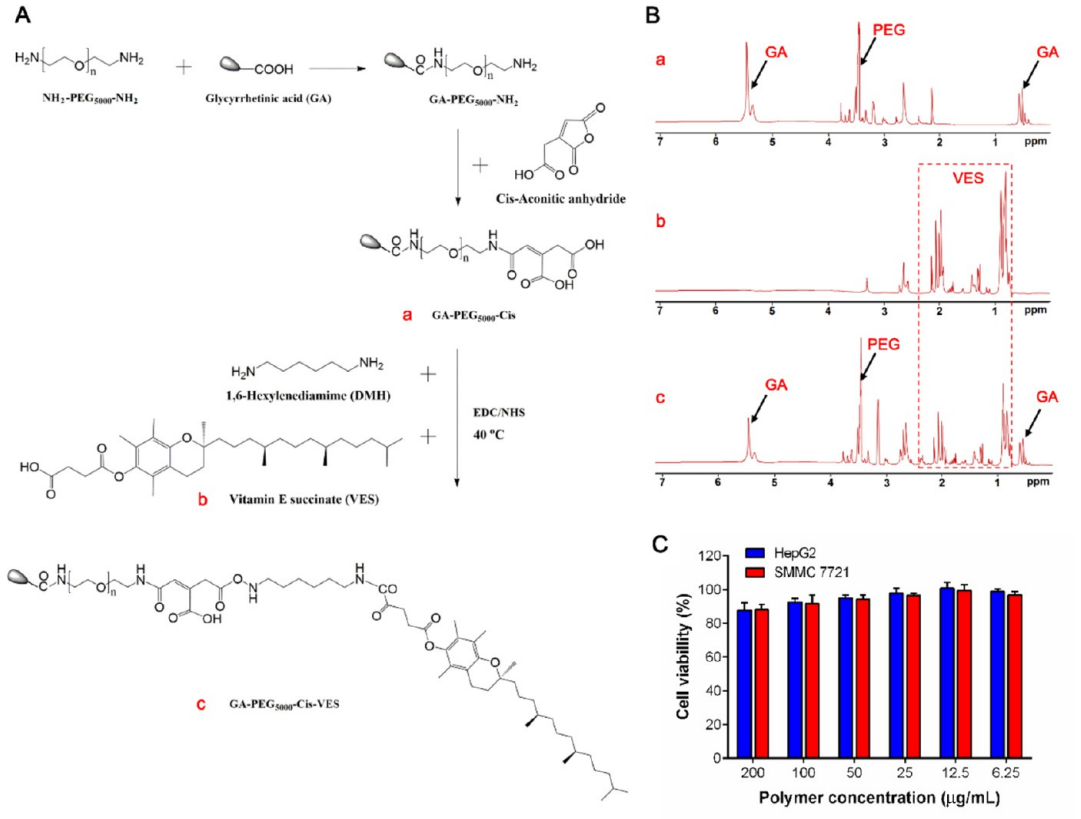

Figure 1. Synthesis and characterization of GA-PEG$_{5k}$-Cis-VES copolymer. (A) Synthetic route of GA-PEG$_{5k}$-Cis-VES (GA-P$_{5k}$CV) copolymer; (B) ^{1}H NMR spectra of GA-PEG$_{5k}$-Cis (a), vitamin E succinate (b), and GA-P$_{5k}$CV (c); (C) cytotoxicity of GA-P$_{5k}$CV copolymer in HepG2 and SMMC 7721 cells after 24 h treatment, evaluated by MTT assay.

administered into mice whose tumor volume was reaching approximately 1000 mm^3. At 6, 12, and 24 h post injection, nude mice were anesthetized by intraperitoneal injection with 2% pentobarbital sodium. At 24 h post injection, mice were sacrificed and the fluorescence intensity imaging of collected organs was recorded. Using the autofluorescence of DOX, fluorescence images of *in vivo* and *ex vivo* tissues were taken at an excitation wavelength of 490 nm and an emission wavelength of 580 nm using the NightOWL LB 983 *in vivo* Imaging System (Berthold Technologies, Germany).

***In Vivo* Antitumor Efficacy.** Liver-tumor-bearing mice were obtained via subcutaneous inoculation with SMMC 7721 cells as above. After 5 days, tumor-bearing mice were randomly assigned to four groups (n = 4): (i) saline, (ii) free DOX, (iii) DOX/non GA@TAT-M, and (iv) DOX/GA@TAT-M (DOX dose of 5 mg/kg).[34,35] Formulations were administered intravenously once every 2 days for 2 weeks. The body weight and tumor volume, calculated with the formula ([width]^2 × [length]/2), were recorded once every 2 days. Then, mice were sacrificed and photographed, and the primary tumors were excised and weighed. The tumor tissues were fixed with 4% (v/v) formaldehyde and sectioned into 6-μm slices. The histologic sections of primary tumor and heart tissues were used for hematoxylin and eosin (H&E) staining to detect apoptosis and necrosis.

Statistical Analysis. All data were presented as the mean ± SD. Statistical significance was assessed by one-way ANOVA. Significant differences between groups were considered at $p < 0.05$.

RESULTS

Synthesis and Characterization of GA-P$_{5K}$CV. P$_{5k}$CV copolymers were able to form stable micelles self-assembly due to its amphiphilic structure of lipophilic alkyl tail and hydrophilic polar head.[36] The P$_{5k}$CV copolymer was designed to be pH-sensitive by the introduction of cis-acotonic anhydride between the PEG moiety and the VES segment. In that case, GA was conjugated to the P$_{5K}$CV in order to guide the micelles to HCC tissue/cells by GA-receptor mediation, and then the copolymer broke down in response to acid environment. The synthesis pathway was illustrated in Figure 1A, and the compositions of GA-PEG$_{5k}$-Cis (a), VES (b), and GA-P$_{5K}$CV(c) copolymers were examined by ^{1}H NMR spectra in $CDCl_3$ (Figure 1B), respectively. The uniform peaks in Figure 1B-a and Figure 1B-c around δ0.6 ppm and δ5.3 ppm indicated the successful conjugation of GA to the P$_{5K}$CV.[15,37] The peaks in Figure 1B-c at δ 3.3−3.6 attributed to the protons from the glycol unit (−CH_2−CH_2−O−) in PEG chain, confirmed that the PEG moiety was involved. The corresponding peaks in the region of 0.7−2.1 ppm (benzyl groups in VES block) in Figure 1B-b and Figure 1B-c may indicate the existence of VES moiety in final products. Moreover, the conjugation ratio of GA in GA-P$_{5k}$CV was measured to be 6.8% by UV−vis spectrophotometry (PerkinElmer, Co., USA) at λ = 250 nm using glycyrrhetinic ammonium salt as standard. Furthermore, this copolymer was highly biocompatible in both HepG2 and SMMC 7721 cells. More than 85% of the cells survived well after treated with 6.25−200 μg/mL GA-P$_{5k}$CV for 24 h (Figure 1C), indicating the GA-P$_{5k}$CV was highly biocompatible.

DOI: 10.1021/acs.molpharmaceut.7b00404
Mol. Pharmaceutics 2017, 14, 3644−3659

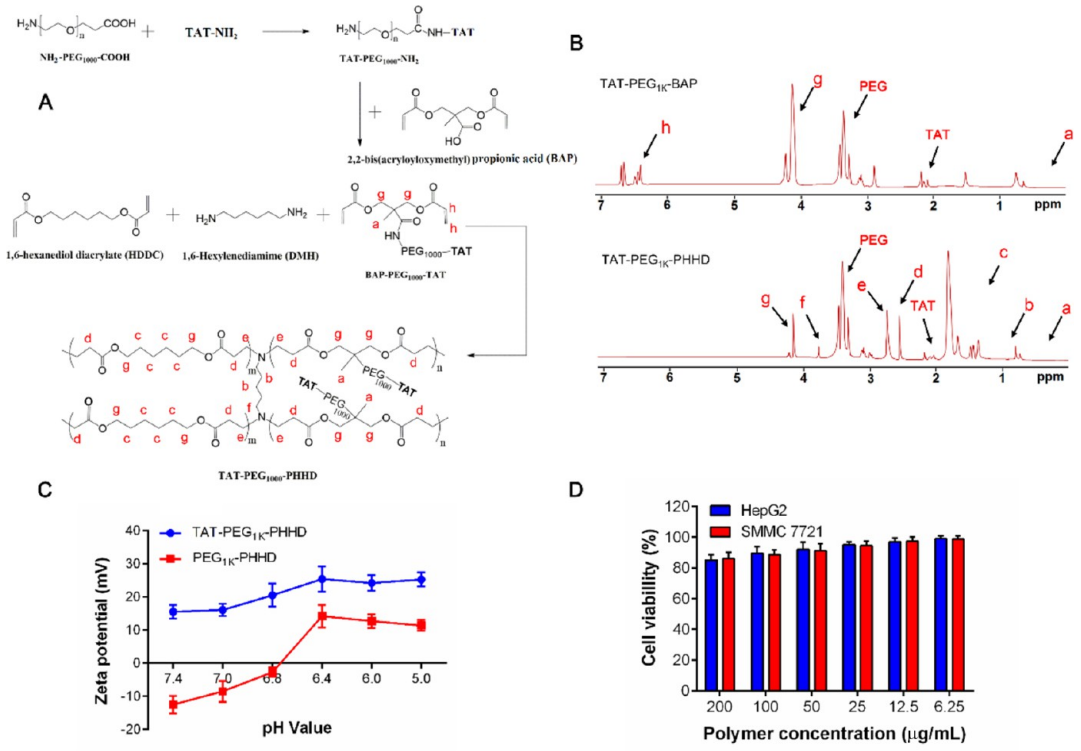

Figure 2. Synthesis and characterization of TAT-PEG_{1k}-PHHD copolymers. (A) Synthetic route of TAT-PEG_{1k}-PHHD copolymer; (B) ^1H NMR spectra of TAT-PEG_{1k}-BAP (a) and TAT-PEG_{1k}-PHHD (b); (C) zeta potential changes of TAT-PEG_{1k}-PHHD and PEG_{1k}-PHHD micelles at different pH values; (D) cytotoxicity of TAT-PEG_{1k}-PHHD copolymer in HepG2 and SMMC 7721 cells after 24 h treatment by MTT assay.

Table 1. Characteristics of DOX-Loaded Micelles Constituted by Various Weight Ratios of GA-P_{5k}CV and TAT-PEG_{1k}-PHHD Polymers

weight ratio (GA-P_{5k}CV: TAT-PEG_{1k}-PHHD)	size (nm)	PDI	zeta potential (mV)	DLE (%)	DEE (%)
5:1	196.25 ± 5.27	0.26 ± 0.04	−24.64 ± 4.62	5.3	37.4
2:1	136.73 ± 3.75	0.31 ± 0.03	−21.51 ± 3.48	8.5	59.6
1:1	118.46 ± 4.25	0.21 ± 0.02	−18.53 ± 2.64	10.8	76.8
1:2	68.97 ± 2.56	0.24 ± 0.02	−16.55 ± 1.32	12.1	86.8
1:5	76.26 ± 2.38	0.17 ± 0.02	−4.34 ± 0.65	12.8	90.5

Synthesis and Characterization of TAT-PEG_{1k}-PHHD. TAT-PEG_{1k}-PHHD was synthesized via Michael addition reaction.[38,39] In this synthesis route (Figure 2A), TAT was conjugated with PEG_{1k} first, and then conjugated with BAP by amide bond. Three moieties with acrylate group were polymerized together using 1,4-addition reaction among the terminal amine of DMH and acrylate groups of TAT-PEG-BAP, and 1,6-hexanediol diacrylate HDDC. The HDDC moiety was used as the hydrophobic segment in TAT-PEG_{1k}-PHHD polymer. The linear poly(β-amine ester) polymer were most commonly used as drug or genes carriers,[40,41] but the branched structure was more stable and had higher loading efficiency.[42,43] Thus, herein DMH was utilized as the scaffold during the polymerization process. TAT-PEG_{1k}-PHHD with amphiphilic structure was obtained with the molar ratio of HDDC, DMH, and TAT-PEG_{1k}-BAP to be 1:8:2.

The ^1H NMR spectra of TAT-PEG_{1k}-BAP and TAT-PEG_{1k}-PHHD in $CDCl_3$ were shown in Figure 2B. The typical peaks of acrylate-terminated TAT-PEG_{1k}-BAP appeared at δ 6.4−6.7 ppm and disappeared in TAT-PEG_{1k}-PHHD, resulting from the addition reaction on acrylate group. In contrast, signals derived from the methylene in HDDC and DMH (including peaks b, c, d, e, f) appeared in TAT-PEG_{1k}-PHHD, indicating the successful synthesis. Meanwhile, peaks at δ 2.05−2.2 ppm resulted from the methyl and methylene in TAT peptide could be observed in both TAT-PEG_{1k}-BAP and TAT-PEG_{1k}-PHHD spectra. Furthermore, due to the conjugation of TAT peptide, the zeta potential of TAT-PEG_{1k}-PHHD was +16.2 mV at pH 7.4, which could totally reverse the negative potential of the PEG-PHHD (Figure 2C). The positive potential of TAT-PEG_{1k}-PHHD could enhance the cellular uptake but it was likely to induce undesirable side-effects. To overcome this problem, the TAT ligands were designed to be present in the interlayer before approaching to the tumor sites. Interestingly, following by the drop of pH, the negative potential of PEG_{1k}-PHHD gradually reversed to positive potential due to the protonation of tertiary amine in the PEG_{1k}-PHHD structure. Finally, the cytotoxicity of TAT-PEG_{1k}-PHHD against HepG2 and SMMC 7721 cells was evaluated (Figure 2D). Over 85% of cells still survived after the treatment with 3.12−100 μg/mL TAT-PEG_{1k}-PHHD for 24 h, indicating its good biocompatibility.

Physicochemical Characteristics of DOX-Loaded Mixed micelles. Various weight ratios of GA-P_{5k}CV to TAT-PEG_{1k}-PHHD polymers were employed to load DOX. The physicochemical characteristics of DOX/micelles were shown in Table 1. The increasing of GA-P_{5k}CV ratio leaded to

DOI: 10.1021/acs.molpharmaceut.7b00404
Mol. Pharmaceutics 2017, 14, 3644−3659

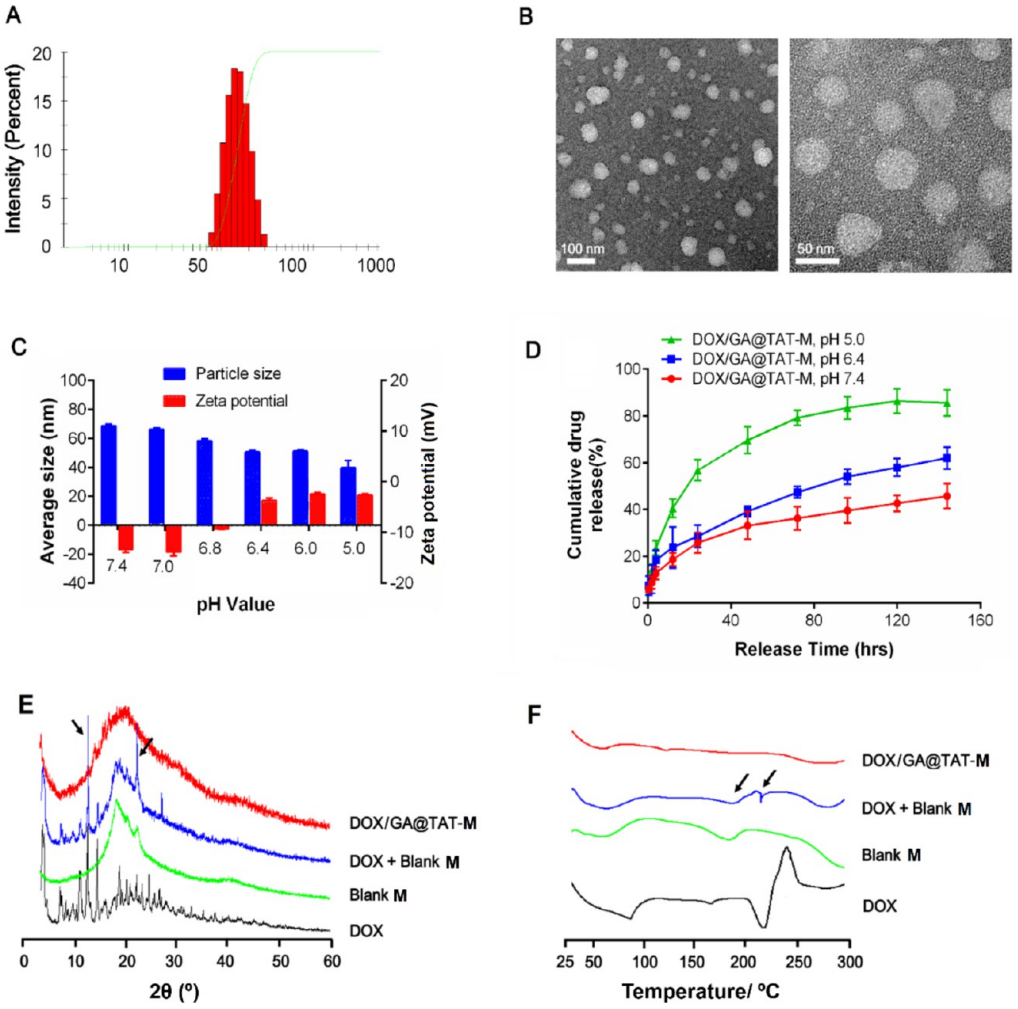

Figure 3. Characterization of DOX/GA@TAT-M composed of GA-PEG$_{5k}$-VES copolymer and TAT-PEG$_{1k}$-PHHD copolymer.(A) Particle size distribution by DLS; (B) TEM images, scale bar was 100 nm (left) and 50 nm (right); (C) average size and zeta potential changes of mixed micelles at different pH values; (D) drug release by DOX/GA@TAT-M *in vitro*; (E) XRD spectra of free DOX, lyophilized blank GA@TAT-M, physical mixture of free DOX and blank GA@TAT-M, and DOX/GA@TAT-M; (F) DSC spectra of free DOX, lyophilized blank GA@TAT-M, physical mixture of free DOX and blank GA@TAT-M, and DOX/GA@TAT-M.

larger particle size, higher absolute value of zeta potential and lower DLE. On the other hand, the increasing ratio of TAT-PEG$_{1k}$-PHHD leaded to DLE sharp increase as a result of the enhanced hydrophobic core, while the zeta potential began to decline because of the charge neutralization by the positive charge of TAT ligands. Therefore, the weight ratio of GA-P$_{5k}$CV:TAT-PEG$_{1k}$-PHHD was optimized to be 1:2 for constituting mixed micelles with DOX encapsulation.

The distribution of particle size (Figure 3A) and TEM images (Figure 3B) revealed that the as-fabricated micelles were uniform and monodispersed at pH 7.4. Figure 3C showed that with pH values dropping, the particle size slightly decreased, and the polarity of zeta potential was reversed at pH 6.4. The P$_{5k}$CV polymer was likely to fracture at pH 6.4 due to the cleaving of the pH-sensitive cis-acotonic anhydride linkage. At the acid environment (pH 5.0−6.4), due to the cleaving of the PEG$_{5k}$ layer from the micelles, the particle size decreased, and the initially shielded TAT ligands in PEG$_{1k}$ moiety were exposed such that the negative zeta potential reversed to be positive. Meanwhile, the different stability resulted from different storage pH values (pH 7.4, 6.4, 5.0) was also conducted. After 1 week storage, there was no significant change on the average particle size of micelles suspension in pH 7.4. However, at day 7 storage, the particle size of micelles in pH 6.4 and pH 5.0 were increased to 135.2 nm (PDI = 0.29) and 295.7 nm (PDI = 0.34), respectively. The remarkable swelling in acid buffer during storage indicated that the fabricated micelles had good storage stability at pH 7.4, while became instable in acid buffer. To investigate the *in vitro* pH-triggered drug release behavior, DOX/GA@TAT-M were incubated in phosphate buffers with different pH, which were used to simulate the normal extracellular milieu (pH 7.4), tumor extracellular environment (pH 6.4), and tumor endosome/lysosome (pH 5.0). As shown in Figure 3C, 45.7 ± 6.2% of DOX was sustainably released from DOX/GA@TAT-M in pH 7.4 buffer over 144 h. Higher amount of DOX was released with a faster rate (62.4 ± 4.7% over 144 h) in pH 6.4, due to the detachment of PEG$_{5k}$ layer and loosening hydrophobic core due to the protonation. Notably, 86.5 ± 5.7% of DOX could be released at pH 5.0 over 144 h, which was likely because the PHHD core reversed to hydrophilicity with higher degree of protonation in pH 5.0. These results supported our hypothesis that the DOX/GA@TAT-M could maintain negative potential and stably encapsulate drugs at pH 7.4, but readily detach the long chain PEG$_{5k}$

DOI: 10.1021/acs.molpharmaceut.7b00404
Mol. Pharmaceutics 2017, 14, 3644−3659

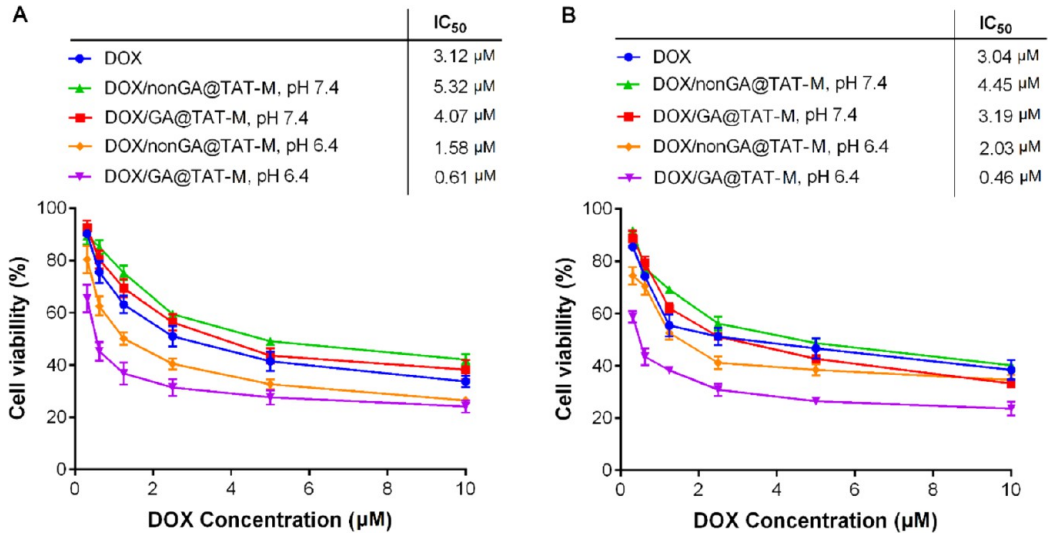

Figure 4. *In vitro* cytotoxicity of various DOX formulations in HepG2 (A) and SMMC 7721 cells (B). IC_{50} values were calculated by GraphPad prism 6.0 software.

shield at acid environment, exposing the TAT peptide on the surface of micelles, and release drugs rapidly at reduced pH.

XRD spectra were conducted to confirm the encapsulation of DOX in the micelles (Figure 3E). Based on its crystalline characteristics, XRD patterns of DOX exhibited sharp peaks at scattered angles ranging from 11° to 14°. Meanwhile, lyophilized blank micelles possessed a sharp peak at 22°. The existence of peaks at 12° and 22° in the physical mixture revealed the crystalline nature of the micelles. No characteristic peaks for DOX in DOX/GA@TAT-M were shown, suggesting the amorphous state of DOX loaded in micelles. Moreover, the thermal behavior of DOX/GA@TAT-M was analyzed with differential scanning calorimetry (DSC) in Figure 3F. The DSC curve of the physical mixture showed a DOX melting peak at 217 °C and another two peaks (at 54.4 °C and at 178 °C) for the blank micelles, where the peak at 178 °C was resulted from the GA ligands in micelles. The presence of the DOX peak at 217 °C for the physical mixture indicated the crystalline state of DOX as free state, while the disappearance of this peak in the DOX/GA@TAT-M suggested the encapsulation of loaded DOX as amorphous structures.

***In Vitro* Cytotoxicity.** The cytotoxicity of DOX/GA@TAT-M and the micelles without GA modification (DOX/nonGA@TAT-M) were tested on HepG2 and SMMC 7721 cells at pH 7.4 or 6.4. After 24 h incubation with the micelles, both DOX/GA@TAT-M and DOX/nonGA@TAT-M at pH 7.4 exhibited relatively lower cytotoxicity in both cell lines, compared to free DOX drugs (Figure 4A and B). Due to the direct intercalation with DNA, the free DOX exhibited higher capacity to kill cells than DOX loaded in nanoparticles. Therefore, at pH 7.4, the DOX loaded in both GA@TAT-M and nonGA@TAT-M exhibited much lower cytotoxicity in normal liver cells than free DOX (Figure S1), indicating its improved biosafety. At pH 6.4, the PEG_{5k} layer was cleaved from the micelles, and the TAT peptides were exposed on micellar surfaces and acted to facilitate cell penetration.[44] In this case, both DOX/GA@TAT-M and DOX/nonGA@TAT-M exhibited much higher cytotoxicity than free DOX or DOX/micelles at pH 7.4. Notably, for the DOX/GA@TAT-M at pH 6.4, the IC_{50} values were over 5-fold smaller than the free DOX.

Cellular Uptake of DOX/Mixed Micelles. To investigate whether the enhanced cytotoxicity of DOX/GA@TAT-M at pH 6.4 was related to pH-triggered TAT activation in acidic medium, the accumulation of DOX (red fluorescence) within cells were traced with FCM and were quantified by measuring the fluorescent intensity. The cellular internalization of DOX/GA@TAT-M and the counterparts including free DOX and DOX/nonGA@TAT-M were tested on SMMC 7721 cells at both pH 7.4 and pH 6.4, for 4 h incubation. As shown in Figure 5A, intracellular DOX accumulation exhibited a time-dependent manner. For free DOX, the internalization rates were similar both at pH 7.4 and pH 6.4, which suggested the cells in pH 6.4 culture medium were intact and their comparative physiological activities were similar to those cultured at pH 7.4. For DOX/micelles, higher cellular uptake was observed at each time point for formulations both at pH 7.4 and pH 6.4. Notably, DOX/GA@TAT-M manifested higher uptake capacity than DOX/nonGA@TAT-M at pH 7.4, which was due to increased endocytosis activities mediated by GA receptors. When the deprotection of longer PEG_{5k} chain occurred at pH 6.4, the TAT peptides were exposed on the surface of micelles, leading up to the significantly enhanced cellular uptake. No remarkable difference was observed between DOX/GA@TAT-M and DOX/non GA@TAT-M at pH 6.4, which was because the effects of the GA ligands on internalization were masked by the potent cell penetration capacity of TAT peptide. Compared to those at pH 7.4, the uptakes at pH 6.4 were enhanced by 2.6-fold, 1.5-fold, and 3.1-fold for 1, 2, and 4 h incubation, respectively. These results suggested that cellular uptake of DOX/GA@TAT-M could be dramatically enhanced by the synergetic effects of liver-targeting of GA receptors and cellular penetration by the exposed pH-triggered TAT.

Furthermore, the potential internalization mechanisms of DOX/GA@TAT-M in SMMC 7721 cells were evaluated at several endocytosis uptake-suppressed condition, including at low temperature, introduction of free GA ligands, or using of endocytic inhibitors (Figure 5B). The uptakes were significantly suppressed at 4 °C, indicating the uptake was likely through energy-dependent endocytosis mechanism. This result was also confirmed by the reduced cellular uptake in the presence of

DOI: 10.1021/acs.molpharmaceut.7b00404
Mol. Pharmaceutics 2017, 14, 3644−3659

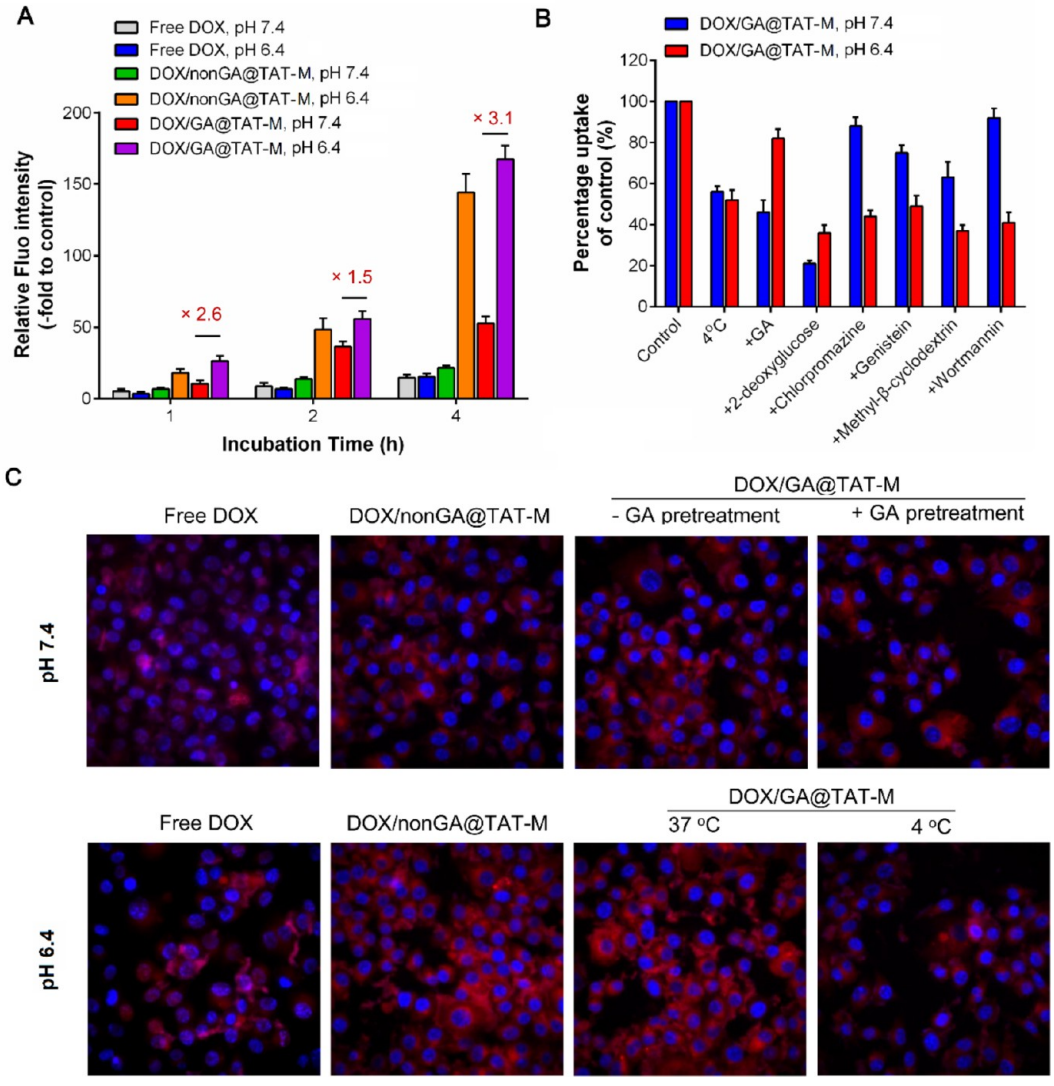

Figure 5. Cellular uptake of various DOX formulations in SMMC 7721 cells. (A) Cellular uptake quantification via fluorescent intensity relative to untreated controls using FCM detection in the PI channel; (B) cellular uptake of DOX/GA@TAT-M in pH 7.4 or pH 6.4 culture medium at 4 °C or following pretreatment for 0.5 h with various endocytic inhibitors at 37 °C; (C) fluorescence microscopy images of the cellular internalization of various DOX formulations under various conditions. (Red-intracellular DOX; blue-Hoechst nuclei staining.)

2-deoxyglucose which inhibited endocytosis.[45] On the other hand, after the cells were pretreated with free GA for 0.5 h, GA receptors on cell surfaces were preoccupied. Over 50% reduction of DOX/GA@TAT-M uptake was observed at pH 7.4, implying the GA receptors could play an important role on mediating the uptake of GA-functionalized micelles. However, this mediation effect became weaker at pH 6.4, which was likely due to the potent activity of TAT peptides. In addition, several typical endocytosis mechanisms were individually inhibited with addition of chemicals. The clathrin- and caveolae-mediated endocytosis were inhibited by chlorpromazine and genistein/m-β-CD, respectively. Macropinocytosis was inhibited by wortmannin to suppress phosphatidylinositol-3-phosphate,[46]. The caveolae-mediated endocytosis mechanism has been revealed to be the main mechanism for GA-functionalized micelles, where the pretreatment of genistein and m-β-CD could result in significant reduction in cellular uptake at pH 7.4 compared to the other counterparts. Nevertheless, cellular uptake of DOX/GA@TAT-M at pH 6.4 was significantly suppressed by all these inhibitors. These results suggested that TAT peptides mediate cellular uptake of the micelles through multiple endocytic pathways.

As shown in Figure 5C, the cellular internalization of various DOX formulations in SMMC 7721 cells was visualized by observing the intracellular autofluorescence of DOX. The intracellular DOX was mainly distributed in cytoplasm. Compared with those at pH 7.4, the amount of DOX was remarkably higher in cells at pH 6.4. Furthermore, much lower intracellular DOX uptake was observed in cells for those pretreated with free GA or at 4 °C (pH 7.4), agreeing with the FCM results.

Mitochondrial Membrane Potential Assay. Mitochondria is one of the primary targets of DOX that results in mitochondria-mediated apoptosis associated with MMP changes. Herein, MMP changes induced by DOX formulations were monitored using fluorescent cationic voltage-dependent dye JC-1. The ratio of green monomer and red aggregate indicated apoptosis degree. After treatment with DOX formulations containing 0.5 μM DOX for 12 h, only DOX loaded micelles at pH 6.4 exhibited more significant MMP decrease in both HepG2 cells (Figure 6A) and SMMC 7721 cells (Figure 6B). Neither DOX/nonGA@TAT-M nor DOX/GA@TAT-M showed obvious MMP changes compared to free DOX at pH 7.4. DOX/GA@TAT-M at pH 6.4 led to dramatic

DOI: 10.1021/acs.molpharmaceut.7b00404
Mol. Pharmaceutics 2017, 14, 3644−3659

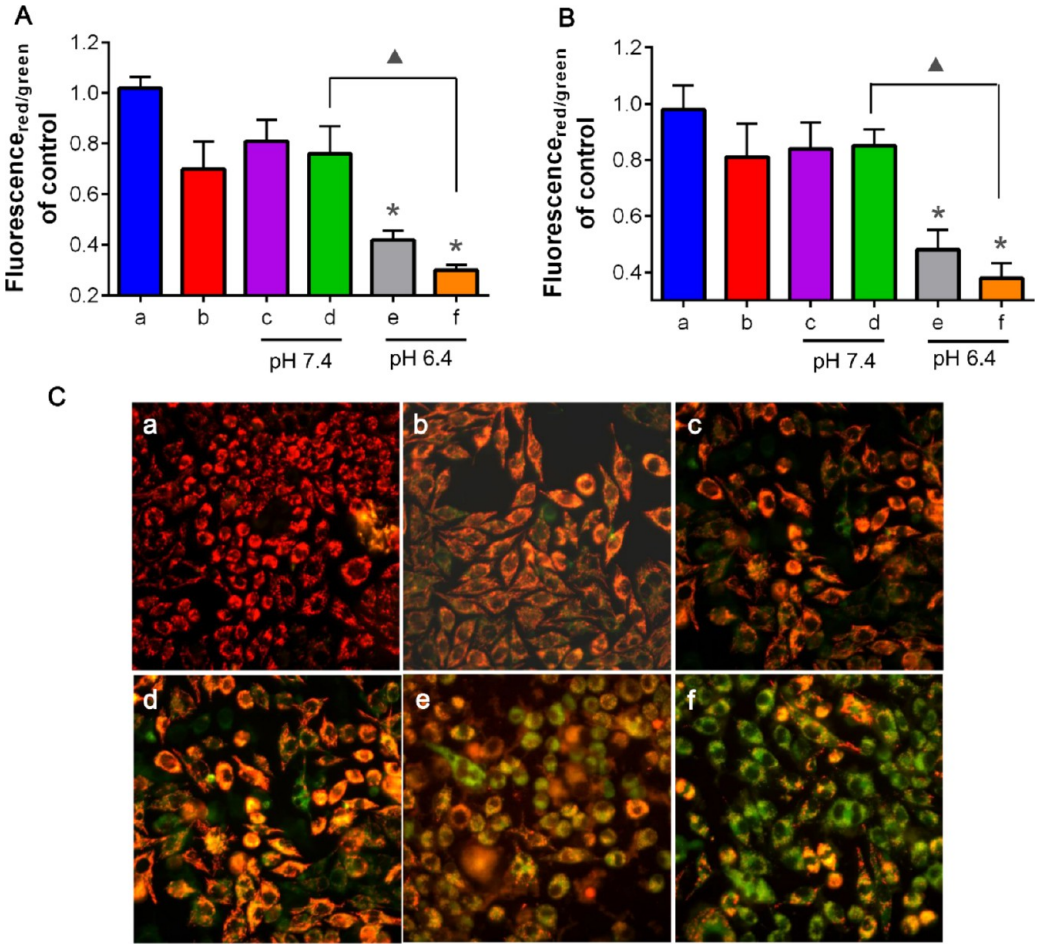

Figure 6. Mitochondrial membrane potential (MMP) changes of HepG2 (A) and SMMC 7721 (B) cells treated by various DOX formulations with equivalent DOX concentration at 0.5 μM for 12 h by JC-1 kit assay. (C) Fluorescence microscopy images of SMMC 7721 cells treated by above-mentioned formulations for 12 h, and then incubated with JC-1 dye for 0.5 h. Red fluorescence repented cells without MMP decline; green fluorescence was produced by the depolarization of MMP and repented cells with early apoptosis. Various (a–f) formulations represented control, blank M, free DOX, DOX/nonGA@TAT-M, and DOX/GA@TAT-M with 0.5 μM DOX at pH 7.4 or pH 6.4. Significant difference between groups illuminated as following: VS free DOX *$p < 0.05$, DOX/GA@TAT-M in pH 6.4 VS in pH 7.4 ▲$p < 0.05$.

MMP reduction compared to those at pH 7.4 ($p < 0.05$). Furthermore, when MMP decreased, red fluorescence generated by JC-1 dye aggregation in mitochondria changed to green fluorescence along with depolarization. The MMP changes in SMMC 7721 cells treated with various formulations were visualized with fluorescence microscopy. Saffron yellow color was the overlay of red and green color. As shown in Figure 6C, few green fluorescence could be observed in the untreated cells. For cells treated with free DOX, DOX/nonGA@TAT-M, or DOX/GA@TAT-M at pH 7.4, green fluorescence generated in cytoplasm due to the MMP decrease. Agreed with the results in Figure 6B, DOX/GA@TAT-M at pH 6.4 induced the most green fluorescence and only little amount of red fluorescence could be observed. These results suggested that the DOX/GA@TAT-M at pH 6.4 could cause early apoptosis against HepG2 and SMMC 7721 cells more effectively than other counterparts.

Intracellular ROS and Apoptosis. DOX has been reported to generate excess amount of ROS, enhance intracellular ROS accumulation, and finally lead to cancer cell death.[47] ROS levels in HepG2 cells and SMMC 7721 cells treated with DOX micelles for 12 h were tested (Figure 7A and Figure 7B). When cells were exposed to 0.5 μM DOX, a slight increase in ROS generation was observed. DOX micelles at pH 6.4 could produce more ROS in comparison with free DOX, agreeing with the results of MMP changes. Although DOX/GA@TAT-M at pH 7.4 did not show higher ROS generation than free DOX, it induced the highest intracellular ROS level at pH 6.4, attributing to the enhanced cellular uptake in acidic environment. Both early apoptotic cells (AnnexinV-FITC^{+ve} PI^{-ve}) and late apoptotic/necrotic cells (AnnexinV-FITC^{+ve} PI^{+ve}) were identified. The total apoptotic cells in HepG2 cell polulation and SMMC 7721 cell population induced by DOX micelles were shown in Figure 7C and D. DOX/GA@TAT-M induced higher apoptosis than those without GA, due to the enhanced cellular uptake by GA receptor mediation. When the DOX/GA@TAT-M were incubated with cells at pH 6.4, it induced higher apoptosis rate in both HepG2 cells and SMMC 7721 cells, resulting in enhanced cytotoxicity and pro-apoptosis activity.

Pharmacokinetics and Biodistribution of DOX/GA@TAT-M. The DOX concentrations in plasma in terms of time after the single injection were shown in Figure 8A and B. The blood circulation time of DOX/GA@TAT-M was significantly extended in comparison to free DOX, with a 4.8-fold longer mean residence time (MRT), 6.7-fold higher area under the curve (AUC), and substantially lower clearance rate (14.2%)

DOI: 10.1021/acs.molpharmaceut.7b00404
Mol. Pharmaceutics 2017, 14, 3644–3659

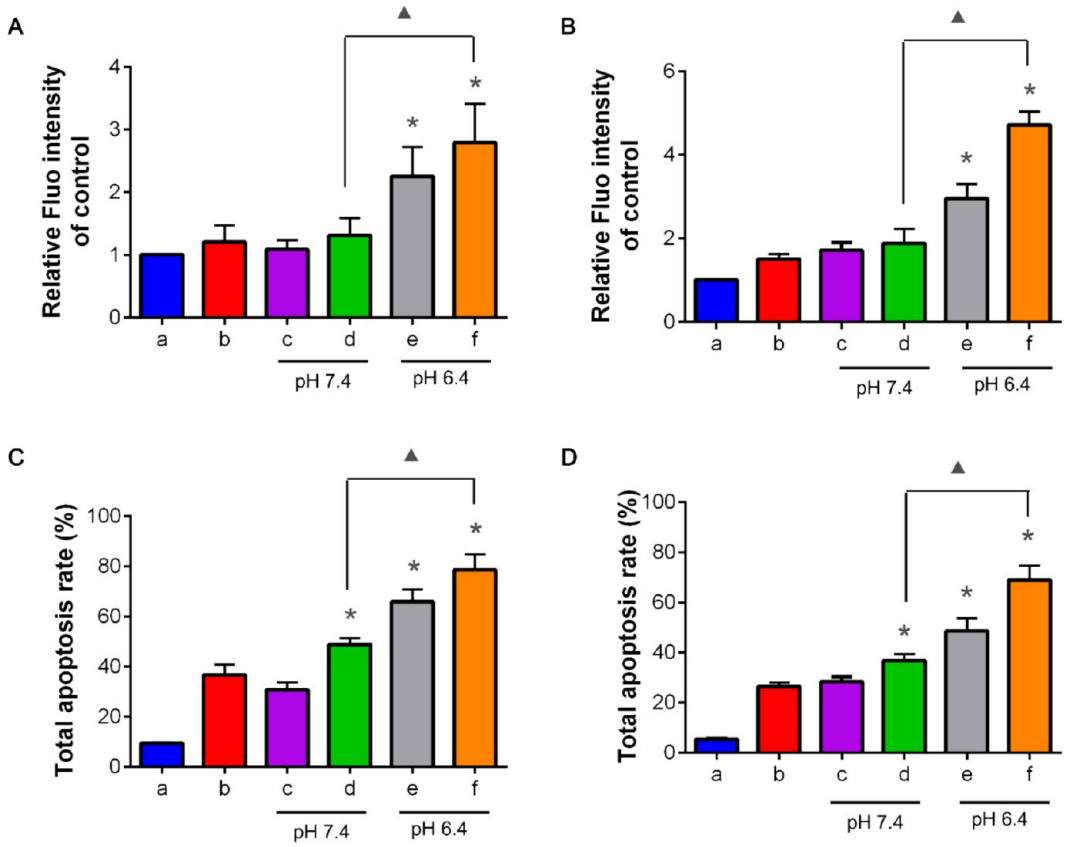

Figure 7. ROS generation of HepG2 (A) and SMMC 7721 cells (B) treated with various DOX formulations with equivalent DOX concentration at 0.5 μM for 12 h by DCFH-DA probe incubation; Annexin V-FITC double staining assay revealing total apoptosis rate including early apoptotic cells (AnnexinV-FITC^{+ve} PI^{-ve}) and late apoptotic/necrotic cells of HepG2 (C) and SMMC 7721 cells (D) treated with various DOX formulations with equivalent DOX concentration of 0.5 μM for 12 h. Various (a–f) formulations represented control, blank M, free DOX, DOX/nonGA@TAT-M, and DOX/GA@TAT-M with 0.5 μM DOX at pH 7.4 or pH 6.4. Significant difference between groups illuminated as following: VS free DOX *$p < 0.05$, DOX/GA@TAT-M in pH 6.4 VS in pH 7.4 ▲$p < 0.05$.

and volume of distribution (24.7%). Although the plasma concentration of free DOX was higher than the DOX/GA@TAT-M during the initial 45 min, its concentration dropped sharply due to rapid clearance. DOX/nonGA@TAT-M exhibited similar PK profiles with DOX/GA@TAT-M, due to the uniform PEGylation and similar particle size.[48] Interestingly, the C_{max} of both free DOX and DOX/nonGA@TAT-M appeared at 1 h postinjection, instead of the first time-point. In our opinion, this result would result from two reasons. First, due to the high lipophilicity of DOX, amounts of DOX would distribute into fatty tissues rapidly after i.v. injection. Later, DOX stored in tissues were released into blood circulation. This phenomenon could be frequently found for some hydrophobic drugs. Additionally, the remarkable C_{max} at 1 h of DOX/nonGA@TAT-M was potentially caused by the encapsulation and sustained-release of DOX loaded in micelles.

To evaluate whether the tissue biodistribution of DOX/GA@TAT-M benefited to antitumor applications and alleviated the cardiotoxicity of DOX, the DOX concentrations in tumor site and heart were monitored at four time points: 0.5, 4, 8, and 12 h. Figure 8C demonstrated that DOX micelles could maintain higher concentration in tumor tissue than free DOX during the tested 12 h period. In particular, after administration of DOX/GA@TAT-M, a high amount of DOX could be detected in tumor, in contrast to micelles without GA modification. It potently demonstrated the HCC-targeting characteristic of GA ligands *in vivo*. A small amount of DOX could be found in the heart, where the DOX delivered through micelles had significantly lower distribution in heart than the free DOX during the initial 8 h. The amount of DOX in heart decreased further at 12 h due to rapid excretion, so that only a very low concentration of DOX (<0.2 μg/g) remained in circulation after 12 h. These results demonstrated that DOX/GA@TAT-M could provide a prolonged circulation, specific tumor targeting and alleviative potential cardiotoxicity.

***In Vivo* and *ex Vivo* Tissue Imaging.** The drug accumulation in tumor-bearing nude mice could be visualized by means of the native red fluorescence of DOX. As shown in Figure 9A, the DOX loaded in GA@TAT-M accumulated in the tumor site as indicated with red circles, and had better tumor targeting distribution than the nonGA@TAT-M and free DOX. Along with the metabolism of DOX, the total fluorescent intensity of DOX in mice administrated with all DOX formulations declined with time. However, for the mice administrated with GA@TAT-M, the fluorescence intensity increased with time in the local tumor site. In contrast, fluorescence in tumor site can be hardly observed for the mice administrated with free DOX or DOX/nonGA@TAT-M. Nevertheless, in tumor of mice with DOX/GA@TAT-M, the intensive fluorescence spot still could be recognized. The *ex vivo* imaging provided quantitative information about the biodistribution of DOX in various tissues without the interference of mice autofluorescence (Figure 9B). In addition, the tumor targeting and prolonged retention properties of DOX/GA@TAT-M could be observed in tumors with more intensive fluorescence even at

DOI: 10.1021/acs.molpharmaceut.7b00404
Mol. Pharmaceutics 2017, 14, 3644–3659

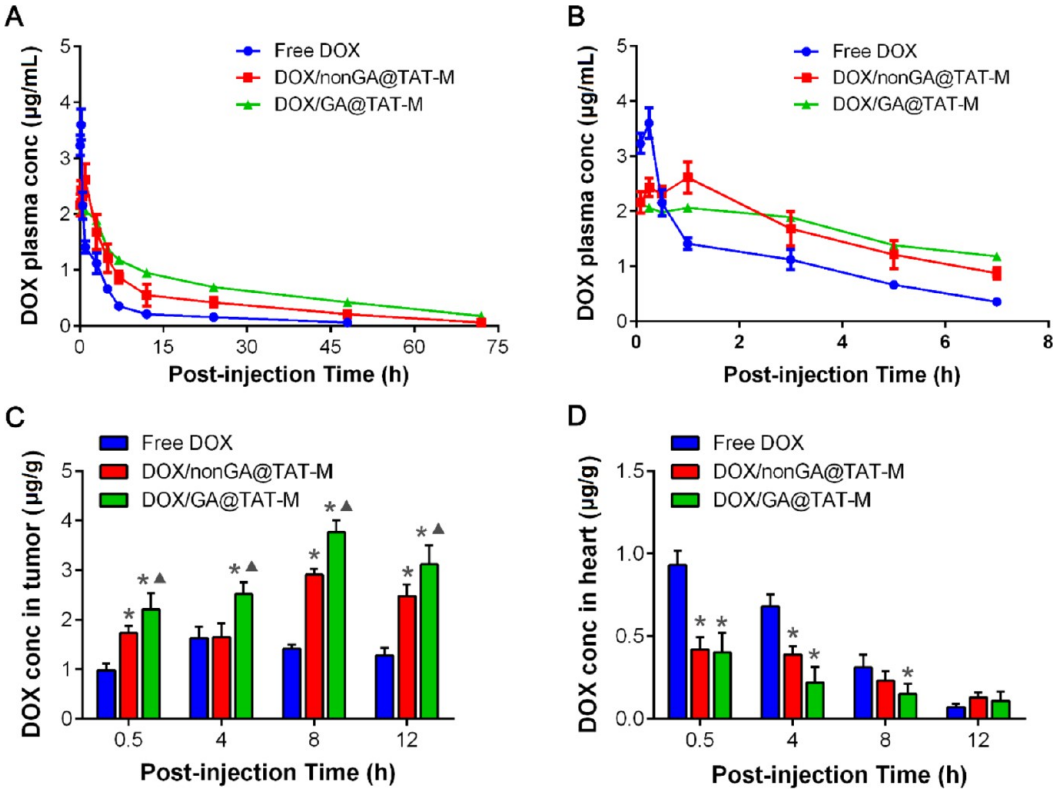

Figure 8. (A) Pharmacokinetic profiles of DOX in tumor-bearing mice after i.v. administration of various DOX formulations at an equivalent dose of 5 mg DOX/kg. DOX was extracted from plasma and measured by LC/MS with daunorubicin as internal control. (B) The magnified pharmacokinetic profiles of DOX in tumor-bearing mice after i.v. administration of various DOX formulations at an equivalent dose of 5 mg DOX/kg inset during initial 7 h; DOX concentrations in tumor (C) and heart (D) at 0.5, 4, 8, and 12 h post injection ($n = 6$). Data were presented as mean ± standard deviation (*$p < 0.05$ VS free DOX, ▲$p < 0.05$ VS DOX/non GA@TAT-M).

24 h postinjection. The *ex vivo* fluorescence intensities in tissues of each group were calculated using indiGO *in vivo* imaging software (Berthold Technologies, Germany) (Figure 9C). The fluorescent intensity of mice treated with DOX/GA@TAT-M was significantly higher than the others at each time point. It was 2.5- (6 h), 2.7- (12 h), and 5.84-fold (24 h) higher compared to those treated with free DOX and 3.64- (6 h), 1.35- (12 h), and 2.36-fold (24 h) higher compared to those treated with DOX/nonGA@TAT-M. This result agreed with the PK profiles above-mentioned, and confirmed the prolonged circulation and specific tumor targeting of DOX/GA@TAT-M.

***In Vivo* Antitumor Efficacy.** The *in vivo* antitumor efficacy and systemic toxicity of DOX/GA@TAT-M were further investigated on HCC-bearing mice. As shown in Figure 10A, tumors in control group grew fast, in which the average tumor volume reached to approximately 1300 mm^3 within 16 days. The treatment of DOX and DOX/nonGA@TAT-M slightly inhibited the tumor growth, in which the final tumor volumes were about 700m^3 and 400 mm^3, respectively. The higher inhibition efficiency of DOX/nonGA@TAT-M compared to saline would be ascribed to the enhanced EPR effect and avoid clearance by endoplasmic reticulum of PEGylated nanocarriers. DOX/GA@TAT-M showed the best antitumor effect with permanent tumor growth inhibition during the whole treatment. The results in Figure 10B indicated that the inhibition efficiency of different treatment groups were: DOX/GA@TAT-M > DOX/nonGA@TAT-M > free DOX, based on the measurement of tumor weight at the end of administration. The tumor tissues in various groups were shown in Figure 10C. The superior tumor growth inhibition effect of DOX/GA@TAT-M might result from the efficient delivery to the tumor site via the synergistic effect of GA receptor targeting and EPR effect, as well as the sufficient intracellular drug release in cancer cells.

The change of bodyweight could indicate systemic toxicity of formulations. Compared to the gently increased bodyweight in the control group, mice treated with free DOX administration showed gradually declined bodyweight (about 20% relative to control group), indicating the toxicity of free DOX (Figure 10D). On the other hand, the treatment with DOX micelles did not cause any significant body weight loss, indicating its little systemic toxicity. The tumor growth inhibition was confirmed via H&E staining (Figure 10E). For saline-treated tumor, well-defined tumor tissues can be clearly seen blue staining cells. Nevertheless, after DOX/GA@TAT-M treatment, only a small portion of tumor tissue stained in blue could be seen, indicating the cancer cell apoptosis. Additionally, the tissue pathological results (Figure 10E) by H&E examination in heart of various treatment groups also indicated DOX/GA@TAT-M possessed lower cardiotoxicity. In heart sections of mice treated by free DOX or DOX/nonGA@TAT-M, myocardial damages could be observed via the loose tissue and destroyed cardiocyte in comparison of control group. However, there was no obvious difference between control group and DOX/GA@TAT-M group. Thus, DOX/GA@TAT-M would be promising in HCC treatment due to the high antitumor efficacy and excellent safety.

DISCUSSION

In view of the respective advantages of active-targeting, TAT-mediated cell penetration and pH-responsive intracellular

DOI: 10.1021/acs.molpharmaceut.7b00404
Mol. Pharmaceutics 2017, 14, 3644−3659

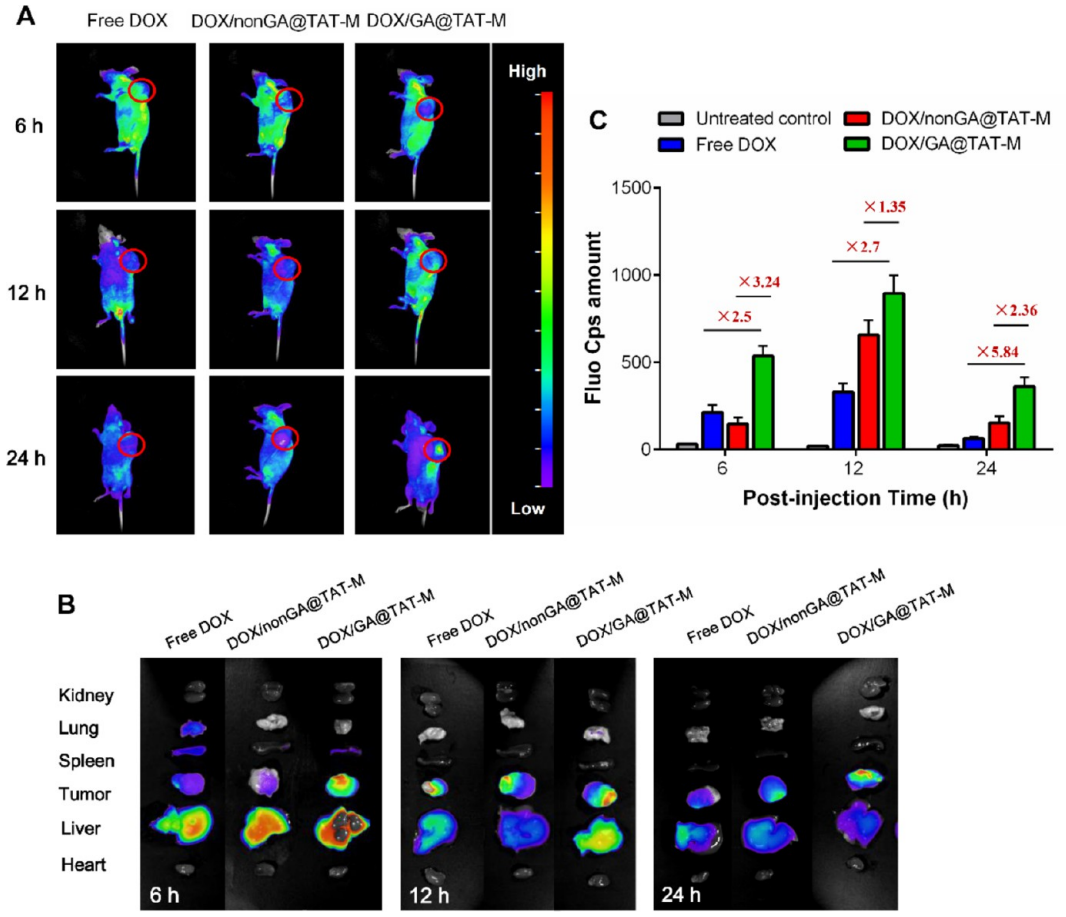

Figure 9. (A) Time-dependent tumor targeting specificity of free DOX, DOX/non GA@TAT-M, and DOX/GA@TAT-M with equivalent concentration of DOX (5 mg/kg), in HepG2 liver tumor-bearing mice (tumor volume about 1000 mm^3, marked by red circle). NIR fluorescence was collected with the excitation wavelength at 490 nm and mission wavelength at 580 nm. (B)Time-dependent biodistribution of DOX in various tissues *ex vivo*. (C) Quantitative fluorescence intensity in tumor at the various time-intervals postinjection with DOX formulations by IndiGo software 2.0 (Berthold Technologies, Germany).

drug release, how to skillfully combine these superiorities would be a challenge for drug delivery in chemotherapy. At present, some studies did attempt to enhance tumor targeting and penetration by dual-ligands modification, commonly, i.e., ligands with selective recognition to tumor and TAT peptides. Zong et al.[49] developed a dual-targeting liposomal system modified with T7 peptide for brain glioma tumor binding and TAT (AYGRKKRRQRRR) for blood-brain barrier penetration. However, there would be design drawback in the mixed micelles composed by DSPE-PEG_{1000}-TAT and DSPE-PEG_{2000}-T7 polymers that part of TAT peptides will be shielded by the long PEG moiety. Similarly, the dual-ligand modified liposomes also confront this dilemma.[50] To overcome this shortage, an activatable drug delivery approach was employed by Koren et al.[51] and Lee et al.,[52] in which TAT peptides were sterically shielded by long PEG moiety containing a degradable pH-sensitive linkage in body circulation. Within the "acidified" milieu in tumor tissue, these carriers would lose the long PEG layer by hydrolysis of pH-sensitive linkers and penetrate internal cells via the activation of TAT peptides exposed on the surface of NPs. Moreover, a stepwise pH-responsive nanoparticle system with HCC targeting, tumor pH charge reversible and "proton-sponge" polymer core was fabricated for dual drugs coloading.[53]

Although there was a significant difference between the groups of DOX/nonGA@TAT-M and DOX/GA@TAT-M at pH 6.4 in Figure 4, there was no significant difference in the cellular uptake result (Figure 5A). In our opinion, the exposed TAT should be the determining factor for the cellular uptake of micelles at pH 6.4. Even so, the results between cellular uptake and cytotoxicity in Figure 4 and Figure 5 were not contradictory. both DOX/nonGA@TAT-M and DOX/GA@TAT-M at pH 6.4 exhibited significantly raised cellular uptake in Figure 5A, compared to that at pH 7.4. Even so, GA ligands also could benefit to recognize the overexpressed receptors on the surface of cancer cells. GA mediated internalization could be demonstrated in Figure 5B. Thus, TAT-M with GA modified still exhibited the enhanced uptake at pH 6.4 in comparison to nonGA@TAT-M after 1, 2, and 4 h incubation, in spite of non-significant difference between them. However, *in vitro* cytotoxicity against cancer cells was not only contributed by the TAT medicated cellular uptake. During 24 h and 48 h treatment, GA receptor medicated endocytosis also promoted micelle internalization. Therefore, in combination of GA ligands and exposed TAT peptides, DOX/GA@TAT-M exhibited higher cytotoxicity against HCC cells.

No doubt, these studies opened our mind and provided us useful drug delivery strategy. In this study, a mixed micelle system was developed to avoid the complicated polymer synthetic process, for example the charge reversible pullulan-based shells were prepared by multistep amide interaction in previous

DOI: 10.1021/acs.molpharmaceut.7b00404
Mol. Pharmaceutics 2017, 14, 3644−3659

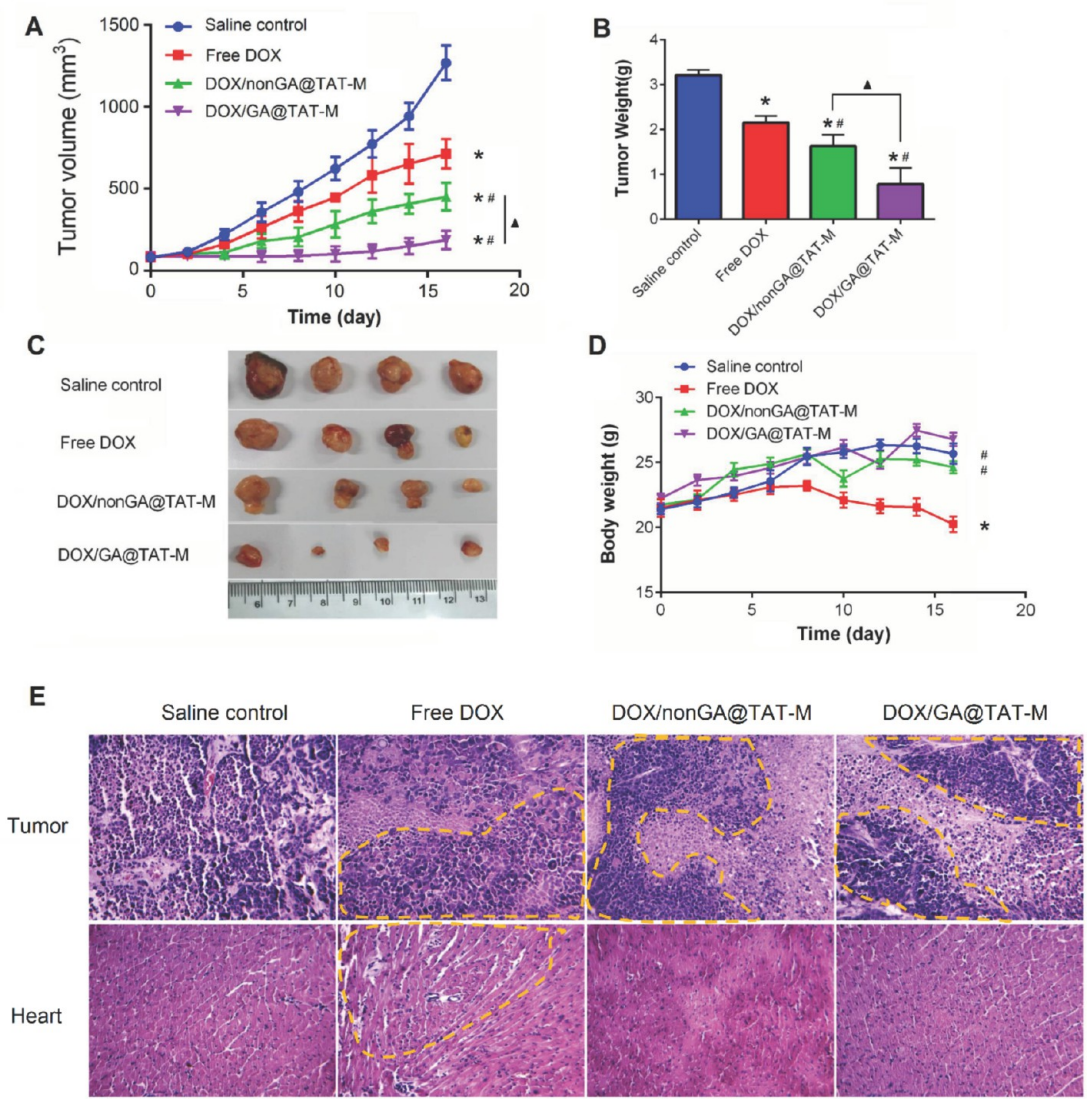

Figure 10. *In vivo* antitumor effect in HepG2 tumor-bearing mice. (A) The variation profiles of tumor volumes during 16 days. (B) Tumor weight at the end of the experiment. (C) Picture of excised tumors at the end of the experiment. (D) The variation profiles of body weight during 16 days. (E) Representative H&E photos of tumors and heart tissues in various groups. Data were given as mean ± SD (n = 5). (*p < 0.05 VS saline control, $^{\#}p$ < 0.05 VS free DOX, ▲p < 0.05 VS DOX/non GA@TAT-M).

report.[53] On the one hand, GA modified long PEG moiety was grafted with hydrophobic VES moiety by pH-sensitive cis-acotonic anhydride linkage in response to the weakly acidic tumor microenvironment (pH ≈ 6.4). Based on the HCC active targeting property of GA ligands and passive targeting by EPR effect, mixed micelles could readily accumulate in tumor tissue. According to the pharmacokinetics and biodistribution results in Figure 8 and Figure 9, GA modified micelles exhibited significantly higher accumulation in tumor and lower distribution in heart than either non-GA modified micelles or free DOX. Furthermore, after GA pretreatment, the cellular uptake of DOX/GA@TAT-M was remarkably decreased (Figure 5), indicating that GA ligands also benefited micelles cellular internalization mediated by the overexpressed receptors on cancer cells. On the other hand, TAT peptides were modified on the short amphiphilic copolymers, i.e., PEG_{1k}-PHHD, in which PHHD possessed the analogous structure with PBAE and exhibited stronger acidic pH-responsive "proton-sponge" character. The shielded TAT peptides could be re-exposed in slightly acid milieu according to the pH value- dependent potential reversal in Figure 2C and Figure 3C. As expected, after coculture in pH 6.4, DOX-loaded mixed micelles could dramatically enter in cancer cells through multiple endocytic pathways (Figure 5). Thus, based on all these contributions, the significantly enhanced anti-HCC efficacy of DOX/GA@TAT-M was observed.

■ CONCLUSION

The multifunctional mixed micelles composed of GA ligand for tumor targeting, TAT peptide for facilitating cellular uptake and acid-triggered drug release were fabricated and applied for DOX delivery for HCC treatment. Specific HCC tissue accumulation and cell internalization of DOX loaded micelles were achieved, and the DOX loaded in PHHD core was apt to escape endo/lysosomal imprison and be released rapidly in cancer cells. The drug release profiles, cancer cells targeting, cellular uptake rate, cellular uptake mechanism, anticancer mechanism, tumor targeting, and antitumor effects were systematically evaluated. This multifunctional mixed micelles provided effective liver targeting, higher anti-HCC efficacy and

DOI: 10.1021/acs.molpharmaceut.7b00404
Mol. Pharmaceutics 2017, 14, 3644−3659

minimized side-effects *in vitro* and *in vivo*. Taken together, the multifunctional nanocarriers provide a promising smart drug delivery approach in HCC treatment.

AUTHOR INFORMATION

Corresponding Authors

* E-mail: suziren@gzucm.edu.cn.
*E-mail: mwchen@umac.mo.

ORCID

Xi Xie: 0000-0001-7406-8444
Meiwan Chen: 0000-0002-8642-5979

Author Contributions

#J.Z. and Y.Z. contributed equally to the work.

Notes

The authors declare no competing financial interest.

ACKNOWLEDGMENTS

This study was supported by the Macao Science and Technology Development Fund (062/2013/A2), the Research Fund of the University of Macau (MYRG2014-00033-ICMS-QRCM, MYRG2014-00051-ICMS-QRCM), and the National Natural Science Foundation of China (81403120).

REFERENCES

(1) Bruix, J.; Sherman, M. Management of hepatocellular carcinoma: an update. *Hepatology* **2011**, *53* (3), 1020−1022.
(2) Singh, S.; Singh, P. P.; Roberts, L. R.; Sanchez, W. Chemopreventive strategies in hepatocellular carcinoma. *Nat. Rev. Gastroenterol. Hepatol.* **2013**, *11* (1), 45−54.
(3) Edeline, J.; Raoul, J.-L.; Vauleon, E.; Guillygomac'h, A.; Boudjema, K.; Boucher, E. Systemic chemotherapy for hepatocellular carcinoma in non-cirrhotic liver: a retrospective study. *WJG* **2009**, *15* (6), 713.
(4) Thomas, M. B.; Zhu, A. X. Hepatocellular carcinoma: the need for progress. *J. Clin. Oncol.* **2005**, *23* (13), 2892−2899.
(5) Davis, M. E.; Shin, D. M.; Chen, Z. Nanoparticle therapeutics: an emerging treatment modality for cancer. *Nat. Rev. Drug Discovery* **2008**, *7* (9), 771−782.
(6) Brannon-Peppas, L.; Blanchette, J. O. Nanoparticle and targeted systems for cancer therapy. *Adv. Drug Delivery Rev.* **2012**, *64*, 206−212.
(7) Soppimath, K. S.; Liu, L. H.; Seow, W. Y.; Liu, S. Q.; Powell, R.; Chan, P.; Yang, Y. Y. Multifunctional core/shell nanoparticles self-assembled from pH-induced thermosensitive polymers for targeted intracellular anticancer drug delivery. *Adv. Funct. Mater.* **2007**, *17* (3), 355−362.
(8) Cheng, R.; Meng, F.; Deng, C.; Klok, H.-A.; Zhong, Z. Dual and multi-stimuli responsive polymeric nanoparticles for programmed site-specific drug delivery. *Biomaterials* **2013**, *34* (14), 3647−3657.
(9) Ganta, S.; Devalapally, H.; Shahiwala, A.; Amiji, M. A review of stimuli-responsive nanocarriers for drug and gene delivery. *J. Controlled Release* **2008**, *126* (3), 187−204.
(10) Yu, B.; Tai, H. C.; Xue, W.; Lee, L. J.; Lee, R. J. Receptor-targeted nanocarriers for therapeutic delivery to cancer. *Mol. Membr. Biol.* **2010**, *27* (7), 286−298.
(11) Zou, Y.; Song, Y.; Yang, W.; Meng, F.; Liu, H.; Zhong, Z. Galactose-installed photo-crosslinked pH-sensitive degradable micelles for active targeting chemotherapy of hepatocellular carcinoma in mice. *J. Controlled Release* **2014**, *193*, 154−161.
(12) Negishi, M.; Irie, A.; Nagata, N.; Ichikawa, A. Specific binding of glycyrrhetinic acid to the rat liver membrane. *Biochim. Biophys. Acta, Biomembr.* **1991**, *1066* (1), 77−82.
(13) Ying, T. H.; Tsai, J. H.; Wu, T. T.; Tsai, M. T.; Su, W. W.; Hsieh, Y. S.; Liu, J. Y. Immunochemical localization of protein kinase C alpha in the biopsies of human hepatocellular carcinoma. *Chin J. Physiol* **2008**, *51* (5), 269−274.
(14) Tian, Q.; Wang, X.; Wang, W.; Zhang, C.; Yuan, Z.; Chen, X. Understanding the role of the C3-hydroxyl group in glycyrrhetinic acid on liver targeting. *J. Controlled Release* **2011**, *152*, e237−e239.
(15) Tian, Q.; Zhang, C.; Wang, X.; Wang, W.; Huang, W.; Cha, R.; Wang, C.; Yuan, Z.; Liu, M.; Wan, H.; Tang, H. Glycyrrhetinic acid-modified chitosan/poly (ethylene glycol) nanoparticles for liver-targeted delivery. *Biomaterials* **2010**, *31* (17), 4748−4756.
(16) Zhang, C.; Wang, W.; Liu, T.; Wu, Y.; Guo, H.; Wang, P.; Tian, Q.; Wang, Y.; Yuan, Z. Doxorubicin-loaded glycyrrhetinic acid-modified alginate nanoparticles for liver tumor chemotherapy. *Biomaterials* **2012**, *33* (7), 2187−2196.
(17) Heldin, C.; Rubin, K.; Pietras, K.; Östman, A. High interstitial fluid pressure-an obstacle in cancer therapy. *Nat. Rev. Cancer* **2004**, *4* (10), 806−813.
(18) Jain, R. K. Vascular and interstitial barriers to delivery of therapeutic agents in tumors. *Cancer Metastasis Rev.* **1990**, *9* (3), 253−266.
(19) Sugahara, K. N.; Teesalu, T.; Karmali, P. P.; Kotamraju, V. R.; Agemy, L.; Girard, O. M.; Hanahan, D.; Mattrey, R. F.; Ruoslahti, E. Tissue-penetrating delivery of compounds and nanoparticles into tumors. *Cancer Cell* **2009**, *16* (6), 510−520.
(20) Kibria, G.; Hatakeyama, H.; Ohga, N.; Hida, K.; Harashima, H. Dual-ligand modification of PEGylated liposomes shows better cell selectivity and efficient gene delivery. *J. Controlled Release* **2011**, *153* (2), 141−148.
(21) Sharma, G.; Modgil, A.; Sun, C.; Singh, J. Grafting of cell-penetrating peptide to receptor-targeted liposomes improves their transfection efficiency and transport across blood-brain barrier model. *J. Pharm. Sci.* **2012**, *101* (7), 2468−2478.
(22) Jiang, Q. Y.; Lai, L. H.; Shen, J.; Wang, Q. Q.; Xu, F. J.; Tang, G. P. Gene delivery to tumor cells by cationic polymeric nanovectors coupled to folic acid and the cell-penetrating peptide octaarginine. *Biomaterials* **2011**, *32* (29), 7253−7262.
(23) Torchilin, V. P. Cell penetrating peptide-modified pharmaceutical nanocarriers for intracellular drug and gene delivery. *Biopolymers* **2008**, *90* (5), 604−610.
(24) Heitz, F.; Morris, M. C.; Divita, G. Twenty years of cell-penetrating peptides: from molecular mechanisms to therapeutics. *Br. J. Pharmacol.* **2009**, *157* (2), 195−206.
(25) Mishra, A.; Lai, G. H.; Schmidt, N. W.; Sun, V. Z.; Rodriguez, A. R.; Tong, R.; Tang, L.; Cheng, J.; Deming, T. J.; Kamei, D. T.; Wong, G. C. L. Translocation of HIV TAT peptide and analogues induced by multiplexed membrane and cytoskeletal interactions. *Proc. Natl. Acad. Sci. U. S. A.* **2011**, *108* (41), 16883−16888.
(26) Berry, C. C. Intracellular delivery of nanoparticles via the HIV-1 tat peptide. *Nanomedicine (London, U. K.)* **2008**, *3* (3), 357−65.
(27) Vivès, E.; Schmidt, J.; Pèlegrin, A. Cell-penetrating and cell-targeting peptides in drug delivery. *Biochim. Biophys. Acta, Rev. Cancer* **2008**, *1786* (2), 126−138.
(28) Delehanty, J. B.; Boeneman, K.; Bradburne, C. E.; Robertson, K.; Bongard, J. E.; Medintz, I. L. Peptides for specific intracellular delivery and targeting of nanoparticles: implications for developing nanoparticle-mediated drug delivery. *Ther. Delivery* **2010**, *1* (3), 411−433.
(29) Kuai, R.; Yuan, W.; Li, W.; Qin, Y.; Tang, J.; Yuan, M.; Fu, L.; Ran, R.; Zhang, Z.; He, Q. Targeted delivery of cargoes into a murine solid tumor by a cell-penetrating peptide and cleavable poly (ethylene glycol) comodified liposomal delivery system via systemic administration. *Mol. Pharmaceutics* **2011**, *8* (6), 2151−2161.
(30) McNeeley, K. M.; Karathanasis, E.; Annapragada, A. V.; Bellamkonda, R. V. Masking and triggered unmasking of targeting ligands on nanocarriers to improve drug delivery to brain tumors. *Biomaterials* **2009**, *30* (23), 3986−3995.
(31) Koren, E.; Apte, A.; Jani, A.; Torchilin, V. P. Multifunctional PEGylated 2C5-immunoliposomes containing pH-sensitive bonds and TAT peptide for enhanced tumor cell internalization and cytotoxicity. *J. Controlled Release* **2012**, *160* (2), 264−273.
(32) Olson, E. S.; Jiang, T.; Aguilera, T. A.; Nguyen, Q. T.; Ellies, L. G.; Scadeng, M.; Tsien, R. Y. Activatable cell penetrating peptides

DOI: 10.1021/acs.molpharmaceut.7b00404
Mol. Pharmaceutics 2017, 14, 3644−3659

linked to nanoparticles as dual probes for in vivo fluorescence and MR imaging of proteases. *Proc. Natl. Acad. Sci. U. S. A.* **2010**, *107* (9), 4311−4316.
(33) Shen, Y.; Tang, H.; Zhan, Y.; Van Kirk, E. A.; Murdoch, W. J. Degradable poly(beta-amino ester) nanoparticles for cancer cytoplasmic drug delivery. *Nanomedicine* **2009**, *5* (2), 192−201.
(34) Lu, J.; Zhao, W.; Huang, Y.; Liu, H.; Marquez, R.; Gibbs, R. B.; Li, J.; Venkataramanan, R.; Xu, L.; Li, S.; Li, S. Targeted delivery of Doxorubicin by folic acid-decorated dual functional nanocarrier. *Mol. Pharmaceutics* **2014**, *11* (11), 4164−78.
(35) Yu, C.; Zhou, Q.; Xiao, F.; Li, Y.; Hu, H.; Wan, Y.; Li, Z.; Yang, X. Enhancing Doxorubicin Delivery toward Tumor by Hydroxyethyl Starch-g-Polylactide Partner Nanocarriers. *ACS Appl. Mater. Interfaces* **2017**, *9* (12), 10481−10493.
(36) Zhang, Z.; Tan, S.; Feng, S.-S. Vitamin E TPGS as a molecular biomaterial for drug delivery. *Biomaterials* **2012**, *33* (19), 4889−4906.
(37) Wu, F.; Xu, T.; Liu, C.; Chen, C.; Song, X.; Zheng, Y.; He, G. Glycyrrhetinic acid-poly (ethylene glycol)-glycyrrhetinic acid tri-block conjugates based self-assembled micelles for hepatic targeted delivery of poorly water soluble drug. *Scientific World Journal* **2013**, *2013*, 913654.
(38) Ko, J.; Park, K.; Kim, Y.-S.; Kim, M. S.; Han, J. K.; Kim, K.; Park, R.-W.; Kim, I.-S.; Song, H. K.; Lee, D. S.; Kwon, I. C. Tumoral acidic extracellular pH targeting of pH-responsive MPEG-poly (β-amino ester) block copolymer micelles for cancer therapy. *J. Controlled Release* **2007**, *123* (2), 109−115.
(39) Yin, Q.; Gao, Y.; Zhang, Z.; Zhang, P.; Li, Y. Bioreducible poly (β-amino esters)/shRNA complex nanoparticles for efficient RNA delivery. *J. Controlled Release* **2011**, *151* (1), 35−44.
(40) Tang, S.; Yin, Q.; Su, J.; Sun, H.; Meng, Q.; Chen, Y.; Chen, L.; Huang, Y.; Gu, W.; Xu, M.; et al. Inhibition of metastasis and growth of breast cancer by pH-sensitive poly (β-amino ester) nanoparticles co-delivering two siRNA and paclitaxel. *Biomaterials* **2015**, *48*, 1−15.
(41) Akinc, A.; Anderson, D. G.; Lynn, D. M.; Langer, R. Synthesis of poly (β-amino ester) s optimized for highly effective gene delivery. *Bioconjugate Chem.* **2003**, *14* (5), 979−988.
(42) Brey, D. M.; Ifkovits, J. L.; Mozia, R. I.; Katz, J. S.; Burdick, J. A. Controlling poly (β-amino ester) network properties through macromer branching. *Acta Biomater.* **2008**, *4* (2), 207−217.
(43) Wu, D.; Liu, Y.; Jiang, X.; He, C.; Goh, S. H.; Leong, K. W. Hyperbranched poly (amino ester) s with different terminal amine groups for DNA delivery. *Biomacromolecules* **2006**, *7* (6), 1879−1883.
(44) Wang, F.; Wang, Y.; Zhang, X.; Zhang, W.; Guo, S.; Jin, F. Recent progress of cell-penetrating peptides as new carriers for intracellular cargo delivery. *J. Controlled Release* **2014**, *174*, 126−136.
(45) Zubris, K. A. V.; Liu, R.; Colby, A.; Schulz, M. D.; Colson, Y. L.; Grinstaff, M. W. In vitro activity of paclitaxel-loaded polymeric expansile nanoparticles in breast cancer cells. *Biomacromolecules* **2013**, *14* (6), 2074−2082.
(46) Zheng, N.; Yin, L.; Song, Z.; Ma, L.; Tang, H.; Gabrielson, N. P.; Lu, H.; Cheng, J. Maximizing gene delivery efficiencies of cationic helical polypeptides via balanced membrane penetration and cellular targeting. *Biomaterials* **2014**, *35* (4), 1302−1314.
(47) Cao, B.; Li, M.; Zha, W.; Zhao, Q.; Gu, R.; Liu, L.; Shi, J.; Zhou, J.; Zhou, F.; Wu, X.; et al. Metabolomic approach to evaluating adriamycin pharmacodynamics and resistance in breast cancer cells. *Metabolomics* **2013**, *9* (5), 960−973.
(48) Ernsting, M. J.; Murakami, M.; Roy, A.; Li, S.-D. Factors controlling the pharmacokinetics, biodistribution and intratumoral penetration of nanoparticles. *J. Controlled Release* **2013**, *172* (3), 782−794.
(49) Zong, T.; Mei, L.; Gao, H.; Shi, K.; Chen, J.; Wang, Y.; Zhang, Q.; Yang, Y.; He, Q. Enhanced glioma targeting and penetration by dual-targeting liposome co-modified with T7 and TAT. *J. Pharm. Sci.* **2014**, *103* (12), 3891−901.
(50) Zhu, Y.; Cheng, L.; Cheng, L.; Huang, F.; Hu, Q.; Li, L.; Tian, C.; Wei, L.; Chen, D. Folate and TAT peptide co-modified liposomes exhibit receptor-dependent highly efficient intracellular transport of payload in vitro and in vivo. *Pharm. Res.* **2014**, *31* (12), 3289−303.
(51) Koren, E.; Apte, A.; Jani, A.; Torchilin, V. P. Multifunctional PEGylated 2C5-immunoliposomes containing pH-sensitive bonds and TAT peptide for enhanced tumor cell internalization and cytotoxicity. *J. Controlled Release* **2012**, *160* (2), 264−73.
(52) Lee, E. S.; Gao, Z.; Kim, D.; Park, K.; Kwon, I. C.; Bae, Y. H. Super pH-sensitive multifunctional polymeric micelle for tumor pH(e) specific TAT exposure and multidrug resistance. *J. Controlled Release* **2008**, *129* (3), 228−36.
(53) Zhang, C.; An, T.; Wang, D.; Wan, G.; Zhang, M.; Wang, H.; Zhang, S.; Li, R.; Yang, X.; Wang, Y. Stepwise pH-responsive nanoparticles containing charge-reversible pullulan-based shells and poly(beta-amino ester)/poly(lactic-co-glycolic acid) cores as carriers of anticancer drugs for combination therapy on hepatocellular carcinoma. *J. Controlled Release* **2016**, *226*, 193−204.

DOI: 10.1021/acs.molpharmaceut.7b00404
Mol. Pharmaceutics 2017, 14, 3644−3659